Luminescent Pt(II) Complexes Featuring Imidazolylidene-Pyridylidene and Dianionic Bipyrazolate: from Fundamentals to OLED Fabrications

Chung-Hao Tseng,[a] Mark A. Fox,[b,*] Jia-Ling Liao,[a] Chia-Hao Ku,[c] Zong-Ting Sie,[c] Chih-Hao Chang,[c,*] Jin-Yun Wang,[d] Zhong-Ning Chen,[d] Gene-Hsiang Lee[e] and Yun Chi[a,*]

[a] Department of Chemistry, National Tsing Hua University, Hsinchu 30013, Taiwan; E-mail: ychi@mx.nthu.edu.tw

[b] Department of Chemistry, Durham University, South Road, Durham, DH1 3LE, UK; E-mail: m.a.fox@durham.ac.uk

[c] Department of Photonics Engineering, Yuan Ze University, Chungli 32003, Taiwan; E-mail: chc@saturn.yzu.edu.tw

[d] Fujian Institute of Research on the Structure of Matter, CAS, State Key Laboratory of Structural Chemistry, China

[e] Instrumentation Center, National Taiwan University, Taipei 10617, Taiwan

For Table of Contents Only

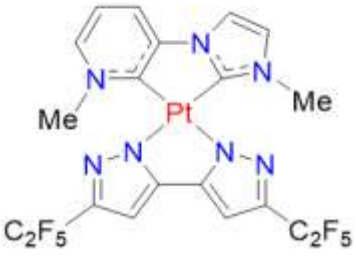

[Pt(Me$_2$impy)(biepz)] (**3**)

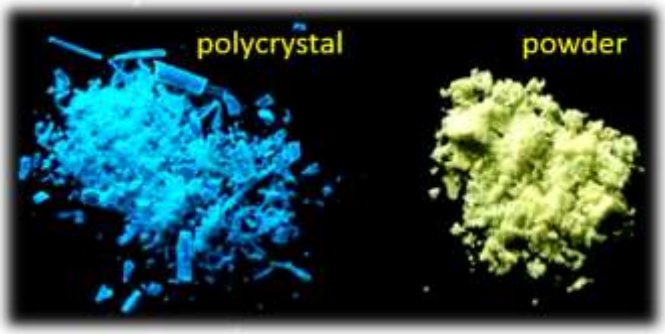

Synopsis:

The photographs of [Pt(Me$_2$impy)(biepz)] (**3**) as polycrystal and powder under UV

irradiation are presented to show the intriguing structural-photophysical behaviors of **3** and related luminescent Pt(II) derivatives in this study.

Abstract

Pt(II) complexes bearing imidazolylidene-pyridylidene (impy) and dianionic biazolate chelates were synthesized, for which the end products depend on the alkyl substituents of the impy chelate. Treatment of $Pt(DMSO)_2Cl_2$ with dimethyl substituted imidazolium-pyridinium pro-ligand $Me_2impy(PF_6)_2$, followed by addition of 5,5'-(1-methylethylidene)-bis-(3-trifluoromethyl-1H-pyrazole) ($mepzH_2$), 5,5'-di(trifluoromethyl)-3,3'-bis-pyrazole ($bipzH_2$), and 5,5'-di(pentafluoroethyl)-3,3'-bis-pyrazole ($biepzH_2$), afforded Pt(II) complexes [Pt(Me_2impy)(mepz)] (**1**), [Pt(Me_2impy)(bipz)] (**2**) and [Pt(Me_2impy)(biepz)] (**3**), respectively. In contrast, reactions with ethyl and isopropyl substituted $Et_2impy(PF_6)_2$ and $Pr_2impy(PF_6)_2$ and with $bipzH_2$ gave [Pt(EtimHpy)(bipz)] (**4**) and [Pt(PrimHpy)(bipz)] (**5**) respectively, where notable alkyl-to-hydrogen transformations on the pyridylidene fragment took place. The reaction of $Pt(DMSO)_2Cl_2$ with $Et_2impy(PF_6)_2$ followed by addition of ($biepzH_2$) gave two products [Pt(Et_2impy)(biepz)] (**6**) and [Pt(EtimHpy)(biepz)] (**7**). Single crystal X-ray diffraction analyses of **1**, **2** and **5** revealed negligible intermolecular Pt···Pt interactions. Hybrid-DFT and TD-DFT computations were carried out on **1**, **2** and **5** to model the observed crystal structures and explain the photophysical data successfully. Organic light emitting diodes (OLEDs) were fabricated from complexes **4** or **5** using a multiple layered device architecture. The associated OLED performances (i.e. η_{max} = 12.5%, 11.2%, η_L = 44.0 cd/A, 40.6 cd/A, and η_P = 28.0 lm/W, 25.8 lm/W for **4** and **5**) confirmed their suitability in serving as potential OLED phosphors.

Introduction

The design and preparation of third-row transition metal based emitters is a major challenge in the development of organic light-emitting diodes (OLEDs) and associated technologies.[1] Platinum(II) metal complexes have been extensively investigated due to their unique square-planar molecular motif, capability of inducing fast singlet-to-triplet intersystem crossing, and tunable luminescence across the whole visible region.[2] A number of efficient Pt(II) phosphors have been developed, which can be classified by the bonding modes of chelates, namely: dianionic tetradentate chelates, and monoanionic tridentate and bidentate chelates. The tetradentate arrangement of chelate is expected to increase the stability and luminescence efficiency, both are key factors for improving the external quantum efficiency (EQE) to the theoretical limit of 20 ~30%.[3] The second and third classes of Pt(II) based OLED phosphors are those bearing one tridentate chelate plus an anionic ancillary,[4] and with two monoanionic bidentate chelates arranged in either homoleptic or heteroleptic coordination mode,[5] respectively. Furthermore, it has been reported that both monomeric and lower energy excimer emission can be detected with adjustment of the sterically encumbered substituent(s) on the peripheral chelates as well as the OLED configurations.[6]

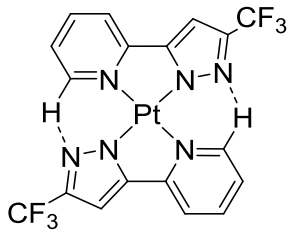

[Pt(fppz)$_2$]

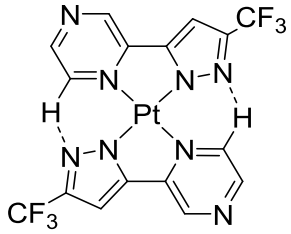

[Pt(fprpz)$_2$]

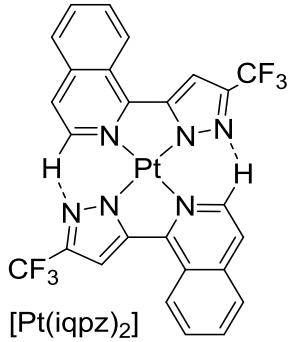

[Pt(iqpz)$_2$]

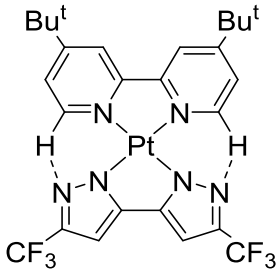

[Pt(btbbpy)(bipz)]

Chart 1. Pt(II) complexes bearing both pyridine and azolate coordination fragments with N···H-C interactions.

Our studies on homoleptic Pt(II) metal complexes bearing two *trans*-oriented functional 2-pyridyl azolates revealed the existence of inter-ligand H-bonding between the pair of adjacent, and non-bonded pyridyl and azolate units, c.f. Chart 1.[7] These N···H-C interactions are known to improve the metal-ligand bond strength and, hence, capable to improve the luminescence even in absence of stronger field chelate with covalent C-Pt interaction.[8] Their planar coordination motif also induced exceedingly strong intermolecular Pt···Pt interaction that eventually afforded the efficient near-infrared (NIR) emission in solid state with remarkable quantum yield (Φ) of 81% as depicted in $[Pt(fprpz)_2]$.[7f] Existence of inter-ligand N···H-C bonding was also confirmed in the relevant Pt(II) complexes bearing both diimine and dianionic biazolate chelates as shown in the second class of Pt(II) complexes represented by [Pr(btbbpy)(bipz)].[9]

In developing new class of Pt(II) based phosphors, we sought to synthesize Pt(II) complexes by replacing diimine with either functional pyridine-carbene[10] or dicarbene chelates.[11] A third option is the imidazolylidene-pyridylidene (Chart 2) which can be generated by deprotonation of imidazolium-pyridinium pro-ligand in the presence of $NaHCO_3$, followed by *in-situ* stabilization with a metal reagent such as $Pt(DMSO)_2Cl_2$. Moreover, the imidazolylidene-pyridylidene chelates are expected to possess much higher-lying π*-orbitals compared to a typical N-heterocyclic carbene,[12] apparently by the reduced π-conjugation, strong σ-donating and weak π-accepting character, thus exemplifying the novelty vs. other Pt(II) complexes. In this paper, we report both of their preparation and intriguing photophysics as solid-state aggregates by both experimental and computational methods. Finally, we describe the fabrication and report the performances of phosphorescent OLEDs using two of these Pt(II) complexes as emitters.

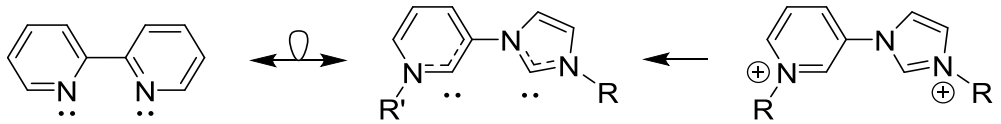

Chart 2. Structural relationship between diimine and imidazolylidene-pyridylidene.

Experimental section:

General Procedures. All reactions were performed under nitrogen. Solvents were distilled over appropriate drying agents prior to use. Commercially available reagents were used without further purification. The 3,3'-bis-pyrazole chelates, i.e. 5,5'-(1-methylethylidene)-bis-(3-trifluoromethyl-1H-pyrazole) ($mepzH_2$), 5,5'-di(trifluoromethyl)-3,3'-bis-pyrazole ($bipzH_2$), and 5,5'-di(pentafluoroethyl)-3,3'-bis-pyrazole ($biepzH_2$) were obtained from Claisen condensation using ethyl trifluoroacetate and 3,3-dimethylpentane-2,4-dione, or employment of ethyl trifluoroacetate or ethyl pentafluoropropionate and 2,3-butanedione, followed by treatment of the obtained β-diketone intermediate with hydrazine hydrate in refluxing ethanol.[9] The imidazolium-pyridinium salts, i.e. 1-methyl-3-(1-methyl-imidazolium-3-yl)-pyridinium diiodide [$Me_2impy(I)_2$], 1-ethyl-3-(1-ethyl-imidazolium-3-yl)-pyridinium diiodide [$Et_2impy(I)_2$] and 1-isopropyl-3-(1-isopropyl-imidazolium-3-yl)-pyridinium diiodide [$Pr_2impy(I)_2$], were prepared by a two-step procedure employing Ullmann coupling of imidazole with 3-bromopyridine, followed by addition of an excess of methyl, ethyl and isopropyl iodide in refluxing acetonitrile, respectively.[13] Anion metathesis using $(NH_4)(PF_6)$ allowed precipitation of $Me_2impy(PF_6)_2$, $Et_2impy(PF_6)_2$ and $Pr_2impy(PF_6)_2$. All reactions were monitored by TLC with pre-coated silica gel plates (Merck, 0.20 mm with fluorescent indicator UV254). Flash column chromatography was carried out using silica gel obtained from Merck (230-400 mesh). Mass spectra were obtained on a JEOL SX-102A instrument operating in electron impact (EI) or fast atom

bombardment (FAB) mode. ^{1}H and ^{19}F NMR spectra were recorded on a Mercury-400 or INOVA-500 instrument. Elemental analysis was carried out with a Heraeus CHN-O Rapid Elementary Analyzer.

Synthesis of [Pt(Me$_2$impy)(mepz)] (1): A mixture of Pt(DMSO)$_2$Cl$_2$ (150 mg, 0.36 mmol), Me$_2$impy(PF$_6$)$_2$ (166 mg, 0.36 mmol) and NaHCO$_3$ (60 mg, 0.73mmol) in 10 mL of DMSO was heated at 110 ^{o}C for 12 h. After then, mepzH$_2$ (122 mg, 0.39 mmol) and NaOAc (146 mg, 1.78 mmol) were added, and the mixture was heated at 110 ^{o}C for another 6 h. Excess of water was next added to induce precipitation. It was filtered and washed with diethyl ether to afford a colorless product. Further purification was conducted by silica gel column chromatography eluting with ethyl acetate. Yield: 166 mg, 69 %. Single crystals of **1** were obtained by diffusion of pentane into a THF solution at RT.

Spectra data of [Pt(Me$_2$impy)(mepz)] (**1**): ^{1}H NMR (500 MHz, d$_6$-DMSO, 298K): δ 8.44 (d, *J* = 6.0 Hz, 1H), 8.23 (d, *J* = 2.0 Hz, 1H), 8.22 (d, *J* = 7.5 Hz, 1H), 7.66 (dd, *J* = 7.5, 6.0 Hz, 1H), 7.51 (d, *J* = 2.0 Hz, 1H), 6.27 (s, 1H), 6.26 (s, 1H), 3.86 (s, 3H), 3.65 (s, 3H), 1.91 (s, 6H). ^{19}F NMR (470 MHz, d$_6$-DMSO, 298 K): δ −58.45 (s, 6F). FAB-MS: m/z 679.6 (M+1). Anal. Calcd. for $C_{21}H_{19}F_6N_7Pt$: C, 37.17; H, 2.82; N, 14.45. Found: C, 37.20; H, 3.06; N, 14.23.

Synthesis of [Pt(Me$_2$impy)(bipz)] (2). Using procedure described for **1**, heating a DMSO solution of Pt(DMSO)$_2$Cl$_2$ (100 mg, 0.23 mmol), Me$_2$impy(PF$_6$)$_2$ (111 mg, 0.24 mmol), NaHCO$_3$ (40 mg, 0.48 mmol) at 150 ^{o}C for 6 hours, followed by treatment with bipzH$_2$ (70.4 mg, 0.26 mmol) and NaOAc (98 mg, 1.2 mmol), afforded yellow [Pt(Me$_2$impy)(bipz)]. Yield: 92 mg, 61 %. Single crystals were obtained from a layered solution of hexane and CH_2Cl_2 at RT.

Spectra data of [Pt(Me$_2$impy)(bipz)] (**2**): ^{1}H NMR (500 MHz, d$_6$-DMSO, 298K): δ 8.59 (d, *J* = 6.5 Hz, 1H), 8.26 (d, *J* = 2.0 Hz, 1H), 8.25 (d, *J* = 8.0 Hz, 1H), 7.72 (dd, *J* = 8.0, 6.5 Hz, 1H), 7.50 (d, *J* = 2.0 Hz, 1H), 6.70 (s, 1H), 6.56 (s, 1H), 4.69 (s, 3H), 4.48 (s,

3H). ^{19}F NMR (470 MHz, d_6-DMSO, 298 K): δ −58.84 (s, CF_3), −59.91 (s, CF_3). FAB-MS: m/z 636.7 $(M)^+$. Anal. Calcd. for $C_{18}H_{13}F_6N_7Pt$: C, 33.97; H, 2.06; N, 15.41. Found: C, 33.82; H, 2.43; N, 15.20.

Synthesis of [Pt(Me_2impy)(biepz)] (3). Using procedure described for **1**, a mixture of $Pt(DMSO)_2Cl_2$ (150 mg, 0.36 mmol), $Me_2impy(PF_6)_2$ (167 mg, 0.36 mmol), $NaHCO_3$ (60 mg, 0.73 mmol) was heated in DMSO, followed by treatment with $biepzH_2$ (144 mg, 0.39 mmol) and NaOAc (146 mg, 1.78 mmol), afforded yellow [Pt(Me_2impy)(biepz)]. Yield: 151 mg, 58 %.

Spectra data of **3**: ^{1}H NMR (500 MHz, d_6-DMSO, 298K): δ 8.61 (d, *J* = 6.0 Hz, 1H), 8.26 (d, *J* = 2.5 Hz, 1H), 8.25 (d, *J* = 8.0 Hz, 1H), 7.72 (dd, *J* = 8.0, 6.0 Hz, 1H), 7.54 (d, *J* = 2.5 Hz, 1H), 6.66 (s, 1H), 6.61 (s, 1H), 4.67 (s, 3H), 4.45 (s, 3H).^{19}F NMR (470 MHz, d_6-DMSO, 298 K): δ −83.20 (s, 3F), −83.37 (s, 3F), −108.10 (s, 2F), −108.83 (s, 2F). FAB-MS: m/z 737.2 (M+1). Anal. Calcd. for $C_{20}H_{13}F_{10}N_7Pt$: C, 32.62; H, 1.78; N, 13.31. Found: C, 32.29; H, 1.79; N, 13.18.

Synthesis of [Pt(EtimHpy)(bipz)] (4). Using procedure described for **1**, heating a DMSO solution of $Pt(DMSO)_2Cl_2$ (150 mg, 0.36 mmol), $Et_2impy(PF_6)_2$ (177 mg, 0.36 mmol), $NaHCO_3$ (60 mg, 0.73 mmol), followed by treatment with $bipzH_2$ (105 mg, 0.39 mmol) and NaOAc (146 mg, 1.78 mmol), afforded light green [Pt(EtimHpy)(bipz)]. Yield: 133 mg, 59 %.

Spectra data of **4**: ^{1}H NMR (500 MHz, d_6-DMSO, 298K): δ 15.80 (br, 1H), 8.65 (t, *J* = 7.0 Hz, 1H), 8.33 (d, *J* = 9.5 Hz, 1H), 8.23 (d, *J* = 2.5 Hz, 1H), 7.70 ~ 7.67 (m, 2H), 6.76 (s, 1H), 6.67 (s, 1H), 5.15 (q, *J* = 8.5 Hz, 2H), 1.39 (t, *J* = 8.5 Hz, 3H). ^{19}F NMR (470 MHz, d_6-DMSO, 298 K): δ −58.99 (s, 3F), −59.03 (s, 3F). FAB-MS: m/z 637.1 (M+1). Anal. Calcd. for $C_{18}H_{13}F_6N_7Pt$: C, 33.97; H, 2.06; N, 15.41. Found: C, 33.95; H, 1.92; N, 15.38.

Synthesis of [Pt(PrimHpy)(bipz)] (5). Using procedure described for **1**, heating a DMSO solution of $Pt(DMSO)_2Cl_2$ (150 mg, 0.36 mmol), $Pr_2impy(PF_6)_2$ (187 mg , 0.36 mmol), $NaHCO_3$ (60 mg, 0.73 mmol), followed by treatment with $bipzH_2$ (105 mg, 0.39 mmol) and NaOAc (146 mg, 1.78 mmol), afforded yellow [Pt(PrimHpy)(bipz)].

Yield: 148 mg, 64 %. Single crystals were obtained from a layered solution of hexane and CH_2Cl_2 at RT.

Spectra data of **5**: ^{1}H NMR (500 MHz, d_6-DMSO, 298K): δ 15.86 (br, 1H), 8.68 (t, *J* = 7.5 Hz, 1H), 8.34 (d, *J* = 10.0 Hz, 1H), 8.30 (d, *J* = 2.5 Hz, 1H), 7.88 (d, *J* = 2.5 Hz, 1H), 7.71 ~ 7.67 (m, 1H), 6.88 (septet, *J* = 8.5 Hz, 1H), 6.78 (s, 1H), 6.69 (s, 1H), 1.48 (d, *J* = 8.5 Hz, 6H).^{19}F NMR (470 MHz, d_6-DMSO, 298 K): δ −59.44 (s, 3F), −59.65 (s, 3F). FAB-MS: m/z 650.6 (M). Anal. Calcd. for $C_{19}H_{15}F_6N_7Pt$: C, 35.08; H, 2.32; N, 15.07. Found: C, 34.80; H, 2.37; N, 15.35.

Synthesis of [Pt(Et_2impy)(biepz)] (6) and [Pt(EtimHpy)(biepz)] (7). Using the procedure described for **1**, heating a DMSO solution of $Pt(DMSO)_2Cl_2$ (150 mg, 0.36 mmol), $Et_2impy(PF_6)_2$ (177 mg, 0.36 mmol), $NaHCO_3$ (60 mg, 0.73 mmol) at 150 ^{o}C for 6 hours, followed by treatment with $biepzH_2$ (144 mg, 0.39 mmol) and NaOAc (146 mg, 1.78 mmol), afforded yellow [Pt(Et_2impy)(biepz)] (**6**) and greenish-yellow Pt(EtimHpy)(biepz)] (**7**). Yield: 35 mg, 13 % for **6** and 140 mg, 55 % for **7**.

Spectra data of **6**: ^{1}H NMR (500 MHz, d_6-DMSO, 298K): δ 8.73 (d, *J* = 7.0 Hz, 1H), 8.30 (d, *J* = 3.0 Hz, 1H), 8.28 (d, *J* = 8.0 Hz, 1H), 7.79 ~ 7.75 (m, 1H), 7.66 (d, *J* = 3.0 Hz, 1H), 6.66 (s, 1H), 6.62 (s, 1H), 5.36 (q, *J* = 9.0 Hz, 2H), 5.15 (q, *J* = 9.0 Hz, 2H), 1.36 (m, 6H).^{19}F NMR (470 MHz, d_6-DMSO, 298 K): δ −83.24 (s, 3F), −83.25 (s, 3F), −108.52 (s, 2F), −108.80 (s, 2F). FAB-MS: m/z 764.5 (M). Anal. Calcd. for $C_{22}H_{17}F_{10}N_7Pt$: C, 34.56; H, 2.24; N, 12.83. Found: C, 34.55; H, 2.30; N, 12.80.

Spectra data of **7**: ^{1}H NMR (500 MHz, d_6-DMSO, 298K): δ 15.91 (br, 1H), 8.53 (m, 1H), 8.29 (d, *J* = 9.5 Hz, 1H), 8.17 (m, 1H), 7.67 ~ 7.65 (m, 2H), 6.82 (s, 1H), 6.74 (s, 1H), 5.10 (q, *J* = 8.5 Hz, 2H), 1.35 (t, *J* = 8.5 Hz, 3H). ^{19}F NMR (470 MHz, d_6-DMSO, 298 K): δ −83.50 (s, 3F), −82.99 (s, 3F), −107.95 (s, 2F), −108.89 (s, 2F). FAB-MS: m/z 736.5 (M). Anal. Calcd. for $C_{20}H_{13}F_{10}N_7Pt$: C, 32.62; H, 1.78; N, 13.31. Found: C, 32.55; H, 1.91; N, 13.45.

Single Crystal X-Ray Diffraction Studies. Single crystal X-ray diffraction data

were measured on a Bruker SMART Apex CCD diffractometer using Mo radiation (λ = 0.71073 Å). The structural analysis and molecular graphics were obtained using the *SHELXTL* program. CCDC-1519153, 1519154 and 1519155 contain the supplementary crystallographic data of Pt(II) complexes **1**, **2** and **5**, respectively. These data can be obtained free of charge from the Cambridge Crystallographic Data Centre via http://www.ccdc.cam.ac.uk.

Cyclic voltammetry. Cyclic voltammetry (CV) studies were performed using a 620A electrochemical analyzer, CH Instruments Inc. Measurements were carried out in 0.1 M $TBAPF_6/CH_2Cl_2$ solutions with a Pt working electrode for oxidations and in 0.1 M $TBAPF_6$/THF solutions with a Au(Hg) alloy working electrode for reductions. The potentials are reported in volts using the FcH/FcH^+ couple as reference. E_{ap} is defined as the anodic peak potential and E_{cp} as the cathodic peak potential.

Photophysics. Steady-state absorption and emission spectra were recorded by a Hitachi (U-3900) spectrophotometer and an Edinburgh (FLS920) fluorometer, respectively. The quantum yields (Φ) of the titled complexes in solid state were measured using an integrating sphere. Lifetimes were measured by multi-channel scaling (MCS) module with μF900 microsecond flash lamp as the excitation source.

Computational studies. Calculations were performed with the Gaussian 09 program package using the B3LYP functional,[14] the SSD pseudopotential[15] for platinum and the basis set 6-311G** for all other atoms.[16] The Grimme dispersion correction model GD3[17] and the conductor-like polarization continuum model CPCM[18] of CH_2Cl_2 solvent were applied to all calculations, and results analyzed further with GaussSum.[19] Structures obtained were confirmed as true minima by the absence of imaginary frequencies.

TD-DFT computations were carried out on the optimized ground state S_0 geometries to predict their absorption data. The predicted $S_0 \leftarrow T_1$ emission wavelengths were converted from the TD-DFT absorption wavelengths of $S_0 \rightarrow T_1$ on the optimized S_0 geometries using an energy scaling factor of 0.92 to take into

account the expected constant Stokes shift in the platinum complexes. Electronic structure and TD-DFT calculations on optimized T_1 geometries were carried out at the ground states. The predicted emission data from T_1 geometries are uncorrected $S_0 \rightarrow T_1$ absorption values.

OLED Fabrication. Commercial organic materials purchased from Nichem were subjected to temperature-gradient sublimation under high vacuum before thermal evaporation. All the p-type conducting, organic, and metal layers were consecutively deposited onto the ITO-coated glass substrate under a base pressure of < 10^{-6} Torr. The deposition system enabled the fabrication of the complete device structure without breaking the vacuum. The active area was defined by the shadow mask (2 × 2 mm^2). Current density-voltage-luminance characterization was measured using a Keithley 238 current source-measure unit and a Keithley 6485 picoammeter equipped with a calibrated Si-photodiode. The electroluminescent spectra were recorded using an Ocean Optics spectrometer.

Results and Discussion

Syntheses and Characterization. Three imidazolium-pyridinium pro-ligands with distinctive alkyl substituents, i.e. $Me_2impy(PF_6)_2$, $Et_2impy(PF_6)_2$, $Pr_2impy(PF_6)_2$, were prepared from Ullmann coupling of imidazole and 3-bromopyridine, addition of methyl, ethyl or isopropyl iodide and, metathesis with hexafluorophosphate following literature method (Scheme 1).[13] Preparation of the heteroleptic Pt(II) complexes using both imidazolium-pyridinium pro-chelate and dianionic biazolates involves a two-step process. First, the impy pro-ligand is treated with $Pt(DMSO)_2Cl_2$ in presence of $NaHCO_3$ to afford the hypothetical intermediates [Pt(impy)Cl_2], impy = imidazolylidene-pyridylidene (impy), which can be collected as colorless powder upon addition of excess of water and characterized using ^{1}H NMR spectroscopies. However, for typical manipulation, the DMSO solution of intermediate was directly treated with various 3,3'-bis-pyrazoles, i.e.

5,5'-(1-methylethylidene)-bis-(3-trifluoromethyl-1H-pyrazole) ($mepzH_2$), 5,5'-di(trifluoromethyl)-3,3'-bis-pyrazole ($bipzH_2$), and 5,5'-di(pentafluoroethyl)-3,3'-bis-pyrazole ($biepzH_2$) in presence of sodium acetate. To our surprise, two classes of distinctive Pt(II) complexes, both with square-planar Pt(II) core geometries, were isolated with either alkyl or hydrogen atom residing on the pyridylidene fragment.

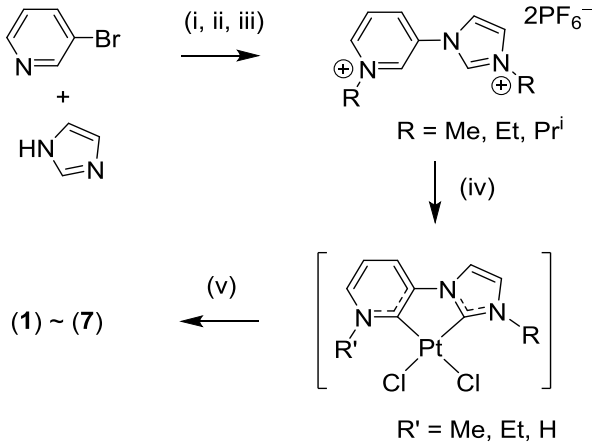

Scheme 1. Generalized synthetic protocols: (i) $CuSO_4$, K_2CO_3, 150 °C; (ii) RI (R = Et or Pr^i), MeCN, reflux; (iii) NH_4PF_6, RT; (iv) $Pt(DMSO)_2Cl_2$, $NaHCO_3$, 110 °C; (v) chelate, NaOAc, 110 °C.

Specifically, the reaction of $Pt(DMSO)_2Cl_2$ with methyl substituted $Me_2impy(PF_6)_2$ resulted in retention of both methyl substituents on impy chelate, i.e. giving formation of [Pt(Me_2impy)(mepz)] (**1**), [Pt(Me_2impy)(bipz)] (**2**) and [Pt(Me_2impy)(biepz)] (**3**), after addition of dianionic bipyrazole chelates; $mepzH_2$, $bipzH_2$, and $biepzH_2$ respectively. In sharp contrast, the reactions of $Et_2impy(PF_6)_2$ and $Pr_2impy(PF_6)_2$, with $Pt(DMSO)_2Cl_2$ and $bipzH_2$ gave formation of a second class of Pt(II) complexes [Pt(EtimHpy)(bipz)] (**4**) and [Pt(PrimHpy)(bipz)] (**5**) respectively, where the alkyl substituent on pyridylidene was transformed to a hydrogen atom. This product selectivity seems to be highly dependent on the both impy chelate and dianionic bipyrazoles, which is evidenced by the isolation of both Pt(II) derivatives

[Pt(Et_2impy)(biepz)] (**6**) and Pt(EtimHpy)(biepz)] (**7**), upon employment of Et_2impy$(PF_6)_2$ and C_2F_5 substituted bipyrazole biepzH_2. Their structural drawings are depicted in Scheme 2 for scrutiny.

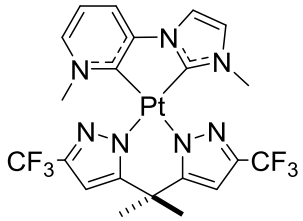

(**1**)

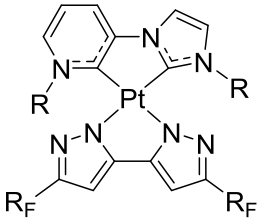

(**2**): R = Me; R_F = CF_3
(**3**): R = Me; R_F = C_2F_5
(**6**): R = Et; R_F = C_2F_5

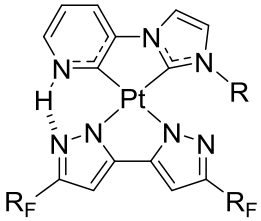

(**4**): R = Et; R_F = CF_3
(**5**): R = Pr^i; R_F = CF_3
(**7**): R = Et; R_F = C_2F_5

Scheme 2. Structural drawings of the studied Pt(II) metal complexes **1** - **7**.

All Pt(II) complexes **1** - **7** were found to be stable in solution and in air, hence, they can be purified by column chromatography, and characterized by mass spectrometry, ^{1}H and ^{19}F NMR spectroscopies, and elemental analyses. Importantly, the dialkyl substituted Pt(II) complexes **1** ~ **3** and **6** showed two sets of alkyl signals in ^{1}H NMR spectra, as two equal intensity singlets in the region of δ 4.69 ~ 3.65 for the dimethyl substituted Pt(II) complexes **1** ~ **3**, and two quartets at δ 5.36 ~ 5.13 for the methylene groups of **6** and an unresolved multiplet at δ 1.36 corresponding to the CH_3 resonance signals of ethyl groups. These features show good agreement with their asymmetric structures. In sharp contrast, Pt(II) complexes **4**, **5** and **7** exhibited only one set of the alkyl signal, together with a single downfield signal at δ 15.80, 15.86 and 15.91 in polar d_6-DMSO solution, respectively. Undoubtedly, one alkyl group has converted to a hydrogen atom responsible for this unique proton signal where an exceedingly strong inter-ligand N···H-C bond is present. The isopropyl substituent of the Pt(II) metal complex **5** exhibits a septet at δ 6.88 assigned to the CH group of isopropyl group which is also considerably downfield to that of the pro-chelate Pr_2impy$(PF_6)_2$, with a chemical shift of δ ~4.80 due to the existence of

the inter-ligand H-bonding interaction in **5**.

Single crystal X-ray diffraction studies on **1**, **2** and **5** were executed to reveal their exact structure and solid-state packing. Crystal of **1** contains two structurally similar but crystallographically distinctive molecules, together with THF and water solvates, which are located at the interstices of packed molecules. Moreover, the imidazolylidene and pyridylidene unit of Me_2impy chelate showed minor positional disorder for one Pt(II) complex, which is a result of similar shapes between the five and six-membered skeletal arrangement of Me_2impy. Figure 1 depicts one molecule, consisting a V-shaped mepz chelate as well as a bowed-shaped geometry for the Pt(II) metal. The observed Pt-C and Pt-N distances of 1.984(5) and 1.983(4) Å and 2.050(4) and 2.054(4) Å are comparable to the metal-ligand bond distances observed in other NHC carbene and azolate Pt(II) metal complexes.[20] Interestingly, an elongated Pt···Pt distance of 6.571 Å is observed, ruling out any Pt···Pt bonding contact.

Figure 2 exhibits the molecular structure of Pt(II) complex **2**, for which the Me_2impy chelate also show similar positional disorder (not shown here), and the planar arrangement of bipz chelate has pushed both methyl groups of Me_2impy chelate to deviate to one side, producing the similar bowed structural motif. Again, all observed Pt-C and Pt-N bonds of 1.994(6) and 1.992(6) Å and 2.063(5) and 2.058(5) Å are slightly longer than those observed in Pt(II) complex **1**, showing a reduced inter-ligand constraint. Furthermore, the molecules are packed in a zig-zag long chain arrangement with equivalent Pt···Pt contacts of 3.914 Å, for which the observed distance is still too long to be considered non-negligible, the later should have a Pt···Pt distance less than ~3.4 Å, i.e. the sum of van der Waals radii of Pt(II) metal ion.[21]

The molecular structure of **5** is depicted in Figure 3. Due to the reduction of inter-ligand interaction by removal of the isopropyl group on the pyridylidene, there exist two H-bonding interactions between the H-coordinated pyridylidene and adjacent pyrazolate (i.e. N(4)···H(3) = 2.035(4) Å) and between the isopropyl group of

imidazolylidene and the second pyrazolate (c.f. N(7)···H(9) = 2.075(4) Å). Moreover, in contrast to the nearly equal Pt-$C_{carbene}$ distances observed in Pt(II) complexes **1** and **2**, a result of imposed positional disorder, the Pt-$C_{pyridylidene}$ distance of **5** (1.948(5) Å) turns substantially shorter than the Pt-$C_{imidazolylidene}$ distance of 1.994(5) Å. Alternatively, the shortening of Pt-N(5) over Pt-N(6) bond, c.f. 2.037(4) vs. 2.079(5) Å, can be also interpreted using stronger *trans* influence imposed by the relatively stronger Pt-$C_{pyridylidene}$ dative bonding. Finally, due to the planar coordination motif of the metal complex, the structure has a zig-zag arrangement with the intermolecular Pt···Pt contact of 3.902 Å, which is comparable to that observed in **2**. This observation suggests that the remaining single isopropyl group on the peripheral imidazolylidene has substantially lengthened the Pt···Pt distance, despite the perfectly planar molecular geometry.

Alkyl to hydrogen conversion. Efforts have put forth here to account for the remarkable alkyl (i.e. ethyl and isopropyl) to hydrogen transformation observed in the products, **4**, **5** and **7**. Firstly, ^{1}H NMR spectroscopy was used to identify the unstable product mixtures of $Pt(DMSO)_2Cl_2$ with $Me_2impy(PF_6)_2$ and $Pr_2impy(PF_6)_2$ without addition of any dianionic chelate. Two distinctive methyl signals and only one set of isopropyl signal, which coincided with the formation of hypothetical species [$Pt(Me_2impy)Cl_2$] and [$Pt(PrimHpy)Cl_2$] respectively, were detected. Secondly, treatment of $Pt(DMSO)_2Cl_2$ with one equivalents of $Et_2impy(PF_6)_2$ and $biepzH_2$ gave a mixture of **6** and **7** with yields of 53% and 13% for **6** and **7** respectively at 100 ^{o}C but at 150 ^{o}C the yields were 8% and 55% for **6** and **7**. Heating **6** at 180 ^{o}C has led to the exclusive formation of **7** thus alkene elimination can also take place from **6** to **7**.

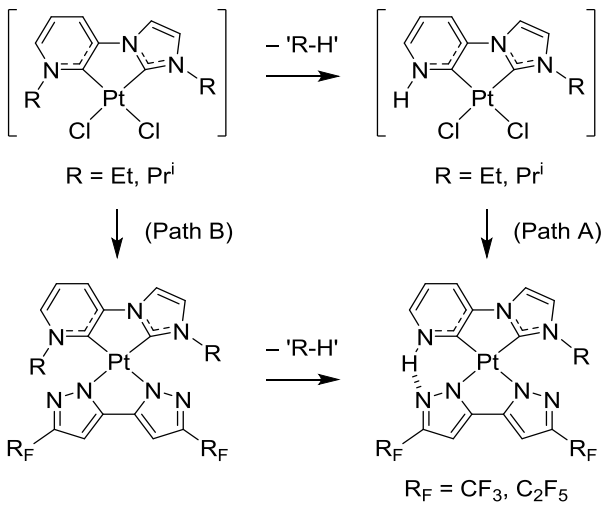

Chart 3. Possible pathways to the formation of Pt(II) complexes **4**, **5** and **7**.

The alkyl to hydrogen transformation by alkene elimination can therefore occur via the formation of Pt(II) intermediate [Pt(RimHpy)Cl_2] (Chart 3, Path A) or after the formation of the expected Pt(II) complex [Pt(R_2impy)(bipz)] (Chart 3, Path B). The chelate Me_2impy displayed no alkyl to hydrogen transformation in the syntheses of **2** and **3** which is attributed to the higher energy barrier of methylene elimination.

Photophysical Properties. Figure 4 depicts UV-Vis absorption spectra of Pt(II) metal complexes **1 – 7** in CH_2Cl_2 at RT, while numerical data are summarized in Table 1. The short wavelength absorptions (< 350 nm) are due to the intra-ligand ππ* transitions, while the long wavelength absorptions between 370 ~ 420 nm could be tentatively assigned to the metal-to-ligand (impy) charge transfer (MLCT) mixed with the ligand-to-ligand charge transfer (LLCT) transitions, i.e. the transition from the filled orbitals of bipyrazolate chelate to the empty π*-orbitals of impy chelate.[22] It is notable that the spectral pattern of **1** is distinctive from all other Pt(II) complexes **2** - **7**, which can be traced to the possession of the unique mepz chelate versus the conjugated bipz and biepz chelates. Moreover, the dialkyl substituted Pt(II) complexes **2**, **3** and **6** display broadened absorptions in the region of 350 ~ 420 nm, which are slightly red-shifted versus the Pt(II) complexes **4**, **5** and **7** with the

H-bonded pyridylidene unit.

All Pt(II) complexes are non-emissive in solution state at RT, such that only the photoluminescence of polycrystals (polycrystalline sample) and powders were measured. The powders were obtained by either vacuum sublimation, grinding of crystalline sample or rapid precipitation from solution state. The efficient solid state emission observed for complexes **1**-**7**, as shown in Table 1, are due to the rigid, solid-state lattices that are capable of destabilizing the metal-centered dd excited states that reduce the non-radiative quenching.[23] As shown in Figure 5, Pt(II) complex **1** showed a featureless emission with peak maximum located at 462 nm, which is independent to the solid morphology, i.e. either as polycrystals or as powders. This result may be attributed to the lack of intermolecular Pt···Pt stacking interaction due to the puckered peripheral arrangement of mepz chelate.

In sharp contrast, the polycrystals of **2** showed a peak maximum at 475 nm, with a longer wavelength shoulder extended down to ~550 nm, this broadened emission profile is due to the co-existence of both segregated and aggregated species as in the polycrystals (Figures 5 and S1(a)). The segregated (monomer) species may have the structure of the Pt_2 dimer separated by the Pt···Pt contact of 3.914 Å, as shown in the previous X-ray structural study. However, after sublimation or rapid precipitation of powder from solution, the peak at 475 nm diminished in intensity, leaving mainly the red-shifted emission with peak maximum at 565 nm, reflecting the assumed strengthening of the Pt···Pt interaction (Figures 5 and S1(b)). Hence, these manipulations may induce the formation of stronger metal-metal-to-ligand charge transfer (MMLCT) process.[24]

The polycrystals of **3** also showed an emission at 466 nm for which the slight blue-shift could be attributed to the more electron-withdrawing C_2F_5 groups in biepz chelate versus the CF_3 substituents in bipz of **2**. Again, after pulverization of sample, the peak at 466 nm diminished in intensity and the main emission is red-shifted to 569 nm (Figure 5 and S1(c)).

The sublimed powder of **6** revealed a broadened emission envelope with maximum at 539 nm, which is considerably blue-shifted compared to both powdered **2** and **3**. This observation can also be understood by the reduced stacking and Pt···Pt interaction imposed by both the bulky Et_2impy and biepz chelates. However, single crystals of **6** could not be obtained to probe the dependence between emission and morphological appearance for **6**.

The emissions of **2** were also recorded in PMMA matrix at RT to confirm the spectral patterns observed in both the polycrystals and powders. As shown in Figure 6, with 2 wt.% of **2** in PMMA the spectrum is identical to that recorded for polycrystals. The band at 475 nm gradually diminished, while the longer wavelength emission band gained intensity upon increasing the doping concentration. At 25 wt.%, the peak profile becomes superimposable to that of powder sample, confirming the occurrence of MMLCT emission expected for the aggregated species. The emissions of **3** in PMMA matrix were not examined due to the relatively poor emission intensities for **3**.

Figure 7 shows the emission spectra of Pt(II) complexes **4**, **5** and **7**, all with the distinctive H-bonded pyridylidene unit. The Pt(II) complex **5** is the only compound where the crystalline form could be obtained. The polycrystalline sample gave an extremely broadened emission profile, alone with shoulder at 470 nm and a peak maximum at 525 nm (Figure S1(d)). After grinding the sample, the emission max. was red-shifted to 535 nm, consistent with the formation of highly aggregated species and, remarkably, both observed and radiative lifetimes were notably reduced to the sub-microsecond range (c.f. Table 1). This tendency may be related to the increased Pt···Pt interaction and enhancement of MMLCT transition character as mentioned earlier.[24a-24i] This property should be advantageous in improving the OLED performances, particularly in searching for the non-doped emitters with higher brightness and reduced emission lifetime, and the OLEDs with the reduced efficiency roll-off at the higher driving voltages.

Both Pt(II) complexes **5** and **7** showed highly similar emission spectra as **2** dispersed in PMMA matrix. At lowered conc. between 2 wt.% and 10 wt.%, there are high energy emissions attributed to the segregated species in PMMA. Interestingly, the presumed segregated (monomer) species of **7** is observed even though the crystalline form of **7** could not be obtained. Nevertheless, the intensity of the high energy emission intensity for **7** is much less than that of **5**. This implies that the higher propensity for **7** to form the aggregated species compared to **5**, due to the reduced steric effect exerted by the smaller ethyl substituent in **7** versus the isopropyl substituent in **5**. The corresponding spectra in PMMA are depicted in Figures S2 and S3 for scrutiny.

Electrochemistry. All Pt(II) complexes **1**-**7** exhibited irreversible oxidation and reduction peaks (Table 1 and Figure S4). The anodic peak potential of the oxidation of **1** at 1.20 V differs considerably from other Pt(II) complexes **2**–**7** at between 0.84 and 0.97 V, which is due to the effect of distinctive dianionic chelates: non-conjugated mepz vs. conjugated bipz and biepz where the π-conjugation of chelate usually reduces the oxidation potential. Furthermore, the trend in the oxidation potentials, **2** (0.84) < **3** (0.86) and **4** (0.90) < **5** (0.94) ~ **7** (0.91), can be understood in terms of the greater electron-withdrawing character of C_2F_5 compared to CF_3 and the slightly increased electron-donating property of the isopropyl group compared to the ethyl group. The cathodic peak potentials are similar for all Pt(II) complexes with a narrow range between –2.12 and –2.23 V and are consistent with impy-centered reductions but other factors responsible for very small differences in the reduction potentials are not obvious.

Computations. Pt(II) complexes **2**, **3** and **6** and complexes **4**, **5** and **7** are distinctive as expected from their molecular geometries (Scheme 2) and the absorption spectroscopic data. As crystal structures were obtained for **2** and **5**, their

geometries are explored computationally as representatives for the two distinct classes along with mepz Pt(II) complex **1**. Optimized geometries for **1** and **5** at B3LYP/SDD:6-311G**/PCM/GD3 reveal good agreements with the experimentally observed structural parameters (cf. Table S1). However, an X-shaped geometry for **2** is favored computationally while a bowed-shaped geometry is observed in the crystal structure of **2** (Figure 8).

An X-shaped geometry based on [Pt(bph)(bpy)] (cf. Chart 3) was computed using model chemistries while a bowed-shaped geometry of [Pt(bph)(bpy)] was determined by X-ray crystallography in a recent study which concluded that crystal packing is responsible for the bowed-shaped geometry.[22a] As **2** and **5** revealed intriguing solid-state emissions, optimized geometries were also carried out for their dimers, $[\mathbf{2}]_2$ and $[\mathbf{5}]_2$, and trimers, $[\mathbf{2}]_3$ and $[\mathbf{5}]_3$, to model the crystal packing interaction observed in these compounds especially for **2** to see if a bowed-shaped geometry is favored over the X-shaped form (Figure 9). It was necessary to include the Grimme dispersion correction (GD3) for realistic modelling of the crystal packing effects here. Without GD3 at B3LYP, the molecules in the dimers and trimers do not stack on optimization.

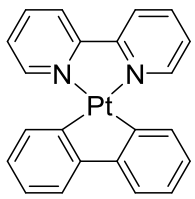

[Pt(bph)(bpy)]

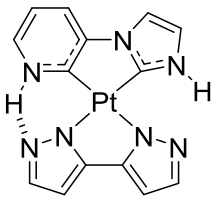

(**8**)

Chart 3. Structural drawing of [Pt(bph)(bpy)] and Pt(II) model complex **8**.

The trimer $[\mathbf{2}]_3$ shows that a bowed molecule of **2** is favored when two molecules of **2** were stacked in contrast to the optimized X-shaped molecule of the monomer **2** (Figures 8 and 9, Table S1). Clearly, the stacking plays an important role in determining its shape. The influence of the bulky isopropyl groups is obvious on going from the monomer **5** to the trimer $[\mathbf{5}]_3$ where the stacking twists the isopropyl

groups away from the neighboring molecule. If the tetramer [**5**]$_4$ (or a larger oligomer) is optimized, the twists in the isopropyl groups would be further reduced and the Pt···Pt distances would lengthen.

Electronic structure calculations reveal little differences in the nature of frontier orbitals for **1**, **2** and **5** where the HOMOs are located on the bipz moieties with some Pt contributions and the LUMOs on the pyridylidene of impy chelate again with some Pt contributions (Figure 10). The % Pt atom contributions for **1**:**2**:**5** are 20:4:7 in the HOMOs and 4:5:3 in the LUMOs (Table S2). Table 2 compares the frontier orbital energies with observed oxidation and reduction potentials from cyclic voltammetry studies. The lower HOMO energy for **1** compared to that for **2** and **5** is reflected in their observed oxidation potentials. There is little difference in the LUMO energies between the three complexes thus the HOMO-LUMO energy gap (HLG) in **1** is larger than HLGs in **2** and **5**.

Predicted photophysical data for the monomer (crystalline) species of **1**, **2** and **5** were obtained by TD-DFT computations on the optimized geometries and important electronic transitions are listed in Table 3. The lowest energy transitions ($S_0 \rightarrow S_1$) are mainly HOMO to LUMO so are the ligand-to-ligand transitions (i.e. from bipz to impy) but, as both frontier orbitals contain some Pt contributions, the transitions should be regarded as mixed metal-ligand to metal-ligand charge transfers (MLMLCT). From Gaussian curve deconvolution analyses on the observed absorption spectra, the fit between calculated and observed lowest energy bands is acceptable (Figure S5 and Table 3). The predicted emission data are based on the assumption that there is little change in the excited state (T_1) with respect to ground state (S_0) geometries and thus the nature of emissions mirror the nature of absorptions. When the Stokes shift energies are factored in, the agreement between observed emission data for the crystalline forms (Figure S6) and computed emission data is very good.

While good agreements between predicted and observed electrochemical and photophysical data have been demonstrated here for the monomer species of **1**, **2**

and **5**, the low energy emissions present in the Pt(II) complexes **2** - **7** are certainly as a result of close interaction(s) between at least two molecules in the solid state. Here, compound (**8**, cf. Chart 3) is looked at as a model monomer for studying the aggregated species present in **2** - **7** to reduce computational efforts since there are many possible dimer geometries that could exist. In the present system, dimers are considered more likely to have stronger intermolecular interactions than trimers and higher oligomers since the intermolecular interactions of one molecule are not 'shared' between two neighboring molecules. The interactions of these dimers thus in turn may be present in the powder for which the lower energy emission bands (or shoulders) were clearly observed.

From sixteen starting dimer geometries of $[\mathbf{8}]_2$ at 45° intervals between the two molecules, geometry optimizations gave nine unique minima, i.e. dimers A – I (Figures 11 and S7). Dimer A has the general conformation found in the crystal structures of **2** and **5**, dimer B with an alternate conformation (one molecule is flipped when compared to A) is the most stable minimum of all and, of particular interest here with respect to low energy emissions, dimer C has the shortest Pt···Pt distance of 3.197 Å.

Electronic structure calculations and TD-DFT predictions on these dimers gave similar data as for the monomer **8** as expected from a recent study on monomers and dimers of platinum(II) complexes.[25] The data here thus do not explain the observed low energy emissions for **2**-**7**. Different computation results have been reported from monomer and dimers for a platinum complex elsewhere but a pure DFT functional (PBE0) was used for TD-DFT on dimer geometries that were optimized at the hybrid DFT functional (B3LYP).[24j] However, use of different model chemistries at DFT and at TD-DFT can lead to misinterpretations of the experimental data. It is assumed here that the T_1 excited state geometries change significantly on excitation of the powdered forms of **2**-**7** to emit such low energy emissions. Unlike closed-shell computations carried out here so far, open-shell computations required for

optimized triplet excited state (T_1) geometries are not considered to be reliable so the following discussions on T_1 geometry data should be treated with some degree of caution.

From the optimized ground state (S_0) geometries for dimers A, B and C as starting geometries, the corresponding triplet excited state (T_1) geometries were optimized. The T_1 geometries revealed subtle geometric changes compared with the S_0 geometries with dimer C computed to be more stable than A and B and its Pt···Pt distance is shortened further by nearly 0.3 Å**.** Electronic structure calculations on T_1 geometries of A and B reveal little changes in the orbital makeups but a different orbital makeup is computed for the T_1 geometry of C. The HOMO in the T_1 geometry of C is largely on both platinum atoms (78% contribution to HOMO) whereas the LUMO is located largely at the pyridylidene fragment with a 7% Pt contribution (Table S3).

TD-DFT data on these T_1 dimer geometries predict the energy emissions of 687, 614 and 594 nm for A, B and C respectively with transitions involving the frontier orbitals. For comparison, a TD-DFT computation on the optimized T_1 geometry of the monomer **8** gives an emission energy of 718 nm. It is difficult to say whether the experimental low energy emissions are exclusively due to Pt···Pt interactions like in dimer C as low energy emissions from other model dimers where the emissions are from MLMLCT states cannot be ruled out computationally here with any certainty. Nevertheless, dimers with close Pt···Pt interactions are likely to exist in the powdered forms of **2** - **7** and the observed low energy emission from each sample may result from the MMLCT excited state. There are indeed many arguments in the literature favoring ^{3}MMLCT in low energy emissions from Pt solids arising from close Pt···Pt interactions especially where such interactions are shown in their experimentally determined structures.[26]

An important point to stress in the computations here is that both S_0 and T_1 dimers here are fully optimized with no symmetry constraints. Some reported

computational studies on geometries of Pt···Pt dimers have constrained the Pt···Pt distances so these geometries could not possibly be true minima.[9, 24i] Optimized geometries of dimers with short Pt···Pt distances can indeed be found by applying an appropriate model chemistry.[27] A more appropriate modeling of strong intermolecular interactions with many more molecules present using a suitable hybrid-DFT model chemistry is desirable along with a polarization model (like the conductor-like polarizable continuum model used for solvent) to give insights into the low energy emissions observed in the solid state from powdered/amorphous forms. Such modeling will take place using superior computational facilities in the future.

OLED Device Fabrication. To investigate the electroluminescent (EL) applications of Pt(II) phosphors **4** and **5**, we fabricated OLEDs using three potential bipolar hosts with adequate triplet energy gaps; namely: 4,4'-N,N'-dicarbazolebiphenyl (CBP),[28] 3-bis(9-carbazolyl)benzene (mCP),[29] and 2,6-bis(3-(9H-carbazol-9-yl)phenyl)pyridine (26DCzppy).[30] In addition, 1,1-bis[(di-4-tolylamino)phenyl]cyclohexane (TAPC) and 1,3,5-tri[(3-pyridyl)-phen-3-yl]benzene (TmPyPB) were chosen as the hole-transport layer (HTL) and the electron-transport layer (ETL) respectively because of their excellent carrier transport abilities and wide triplet energy gaps for achieving exciton confinement.[31] The peak external quantum efficiencies (EQE) of phosphor **4**-based devices with CBP, mCP, and 26DCzppy hosts reached 4.0%, 8.0% and 10.2%, respectively. The superior performance obtained for the 26DCzppy device is due to the endothermic energy transfer and balanced carrier transport; the latter is verified by the large hole and electron mobilities of 2 x 10^{-5} cm^2/Vs reported.[32] However, the turn on voltages of 26DCzppy devices went up to 6.2 V and 5.8 V for phosphors **4** and **5**, which were notably higher than those of mCP or CBP based devices (i.e. ≤ 4 V). This observation can be understood by the higher HOMO of 26DCzppy, which was estimated to be 6.05 eV. Hence, the higher carrier injection barrier between

HTL/EML interface, i.e. between TAPC and 26DCzppy layers, resulted in the higher driving voltage in the 26DCzppy-based OLEDs.

Lowered operating voltages are essential for better performance. Consequently, MoO_3 is incorporated into the hole injection layer to reduce the driving voltages. [33] Architecture of these devices, i.e. A1 and B1, is indicated as follows: ITO/ TAPC with 20 wt.% MoO_3 (20 nm)/ TAPC (40 nm)/ 26DCzppy with 8 wt.% **4** or **5** (20 nm)/ TmPyPB (50 nm)/ LiF (0.8 nm)/ Al (150 nm), where LiF and aluminum serve as the electron injection layer and reflective cathode, respectively. Furthermore, devices with non-doped emitting layer (e.g. devices A2 and B2) were also fabricated to serve as the comparative example.[34] To prevent exciplex formation in both devices A2 and B2, 5 nm-26DCzppy as an electron blocking layer (EBL) was inserted such that the total thickness of HTL+EBL was maintained at 40 nm. Figure 13 presents the structural drawings of the materials used for device assemblies, along with their schematic architectures.

Figure 14 and Table 4 summarize the essential EL characteristics and numerical data of all OLED devices. As depicted in Figure 14(a), the EL spectrum of device A2 using 100 wt.% of **4** was red-shifted by about 40 nm versus the device A1 with 8 wt.% of **4**. Moreover, device A2 had a much larger full width at half maximum (FWHM) of 102 nm, versus ~82.5 nm as recorded for device A1. These results indicate the propensity of **4** in forming relatively more aggregated species in the non-doped thin film.[5c] In contrast, devices B1 and B2, i.e. those fabricated using phosphor **5** at 8 wt.% and 100 wt.%, presented similar EL profile, indicating that the isopropyl group of **5** exerts a greater effect against the aggregate formations versus complex **4** with smaller ethyl substituent.[35] Alternatively, the slightly blue-shifted emission of device B2 versus B1 might be due to the optical interference induced by changing the recombination zone.[36]

As shown in Figure 14(b) and Table 4, the current density-voltage (*J*-*V*) curves revealed that the doped devices with 26DCzppy host exhibited a turn on voltage of

4.6 V, which is lower than the original test device due to the addition of MoO_3 to TAPC. Conversely, both the non-doped devices A2 and B2 revealed a turn-on voltage of 3.6 V. These data probably resulted from the lower band gaps of phosphors **4** and **5**. It is notable that the maximum luminance of device B2 reached 21177 cd/m^2 at 11.6 V, which is slightly higher than that of A2 (i.e. 20679 cd/m^2 at 12.2 V). The EQE of the OLEDs also declined by half at a current density ($J_{1/2}$) of 35.0 and 122.4 mA/cm^2 for devices A2 and B2. Significantly mitigated efficiency roll-off phenomenon obtained in B2 should attributed to the possession of the notably shorter emission lifetime in the solid state which prevents the triplet-triplet annihilation.[37] Furthermore, the charge carrier-exciton interaction may also cause the detected quenching, as the carrier transport has imposed strong influence on both carrier recombination and carrier balance.[38]

As for the doped devices, the maximum luminance of A1 reached 17602 cd/m^2 at 12.0 V, exceeding that of device B1 under identical conditions (i.e. 13844 cd/m^2). Moreover, the $J_{1/2}$ values of devices A1 and B1 were recorded at 41.7 and 33.7 mA/cm^2, respectively. Devices A1 and A2 exhibited similar $J_{1/2}$ values, illustrating that the carrier transport capability of Pt(II) phosphor **4** is comparable to that of 26DCzppy.

Figures 14(c) and 14(d) depicted the diagrams of EQE, luminance and power efficiencies versus luminance, respectively. Both the doped devices A1 and B1 gave peak efficiencies of 12.5% (44.0 cd/A and 28.0 lm/W) and 11.2% (40.6 cd/A and 25.8 lm/W). Moreover, at a practical luminance of 10^3 cd/m^2, device A1 maintained the forward efficiencies of 11.3 %, 39.7 cd/A, and 20.1 lm/W; while those of B1 showed slightly lowered values of 9.4%, 33.8 cd/A, and 17.1 lm/W. Obviously, the small structural difference between **4** and **5** can still influence the carrier balance in the doped EML, allowing the devices A1 and B1 to reach their maxima at distinctive luminance and current densities. Overall, the successful fabrication of OLEDs demonstrated the high potential of these Pt(II) complexes in both display and

lighting applications.

Conclusion.

In conclusion, we have synthesized Pt(II) complexes bearing both functional impy chelate and dianionic biazolate chelates, showing distinctive solid-state photophysical properties that depend on the alkyl substituents of the impy chelate. Of the impy chelate bearing dual methyl substituents, it reacts with the Pt(II) source reagent and dianionic ancillary to form the Pt(II) complexes **1**, **2** and **3**, with retention of both methyl substituents. In sharp contrast, those with ethyl groups afforded both the Pt(II) complex with original chelate structure (i.e. Pt(II) complex **6**) and with the elimination of ethylene and giving formation of H-bonded pyridylidene complexes **4** and **7**, while coupling of isopropyl substituted impy chelate only produced the H-bonded pyridylidene Pt(II) derivative **5**. This observation is consistent with the relative stability of the eliminated hydrocarbon, i.e. propylene > ethylene > methylene.

With the H-bonded pyridylidene chelate, the resulting inter-ligand N···H-C bonding around the Pt(II) metal atom turned the coordination skeleton from puckered to planar, albeit with slightly elongated Pt···Pt distance of ~3.9 Å, as indicated by single crystal X-ray analyses. Furthermore, these Pt(II) complexes showed bright, red-shifted emissions by changing morphologies from crystalline to powder, consistent with the formation of highly aggregated species and, remarkably, both the observed and radiative lifetimes were reduced to the sub-microsecond range. This tendency may be related to the increased intermolecular Pt···Pt interaction and enhancement of MMLCT transition character in powder.

The long Pt···Pt distances and corresponding solid-state stacking of **2** and **5** were successfully reproduced by hybrid DFT computations. The crystalline forms may be regarded as monomers because TD-DFT emission data of monomers of **1**, **2** and **5** are in agreement with the experimental emissions of the polycrystals observed between

462 and 475 nm. The experimental low energy emissions in the powdered forms is likely to derive from dimers with shortened Pt···Pt distances based on the computed model dimer complex $[\mathbf{8}]_2$. The ^{3}MMLCT transitions are most likely to be responsible for these low energy emissions.

Of the four complexes **2**, **4**, **5** and **7** that show strong solid-state emissions, complexes **4** and **5** were selected for practical OLED applications as they are usually in powdered/amorphous forms and made from similar starting materials. Remarkably, multi-layered OLEDs fabricated using complexes **4** or **5** give outstanding device performances, i.e. η_{max} = 12.5%, 11.2%, η_L = 44.0 cd/A, 40.6 cd/A, and η_P = 28.0 lm/W, 25.8 lm/W for **4** and **5**, respectively; confirming their suitability as potential OLED phosphors.

Acknowledgments. This work was supported by the Ministry of Science and Technology of Taiwan, under the grant numbers 101-2113-M-007-013-MY3 and 102-2221-E-155-080-MY3.

Supporting Information Available. Synthetic procedures for various imidazolium-pyridinium salts. X-ray crystallographic data file (CIF) of Pt(II) complexes **1**, **2** and **5**, electrochemical data for all Pt(II) complexes and computational data for complexes **1**, **2**, **5** and **8**. This material is available free of charge via the internet at http://pubs.acs.org.

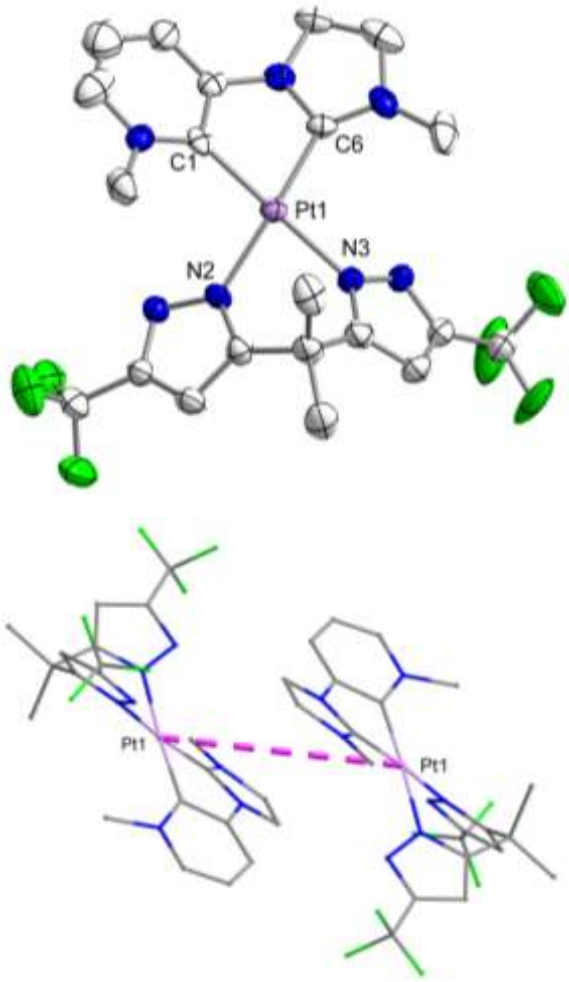

Figure 1. Structural drawing of **1** with thermal ellipsoids shown at the 50% probability level. Diagram showing the molecular stacking and Pt···Pt distance of 6.571 Å. Selected bond distances: Pt(1)-C(1) = 1.984(5), Pt(1)-C(6) = 1.983(4), Pt(1)-N(2) = 2.050(4) and Pt(1)-N(3) = 2.054(4) Å, and bond angles: C(1)-Pt-C(6) = 79.15(19) and N(2)-Pt-N(3) = 82.86(15)°.

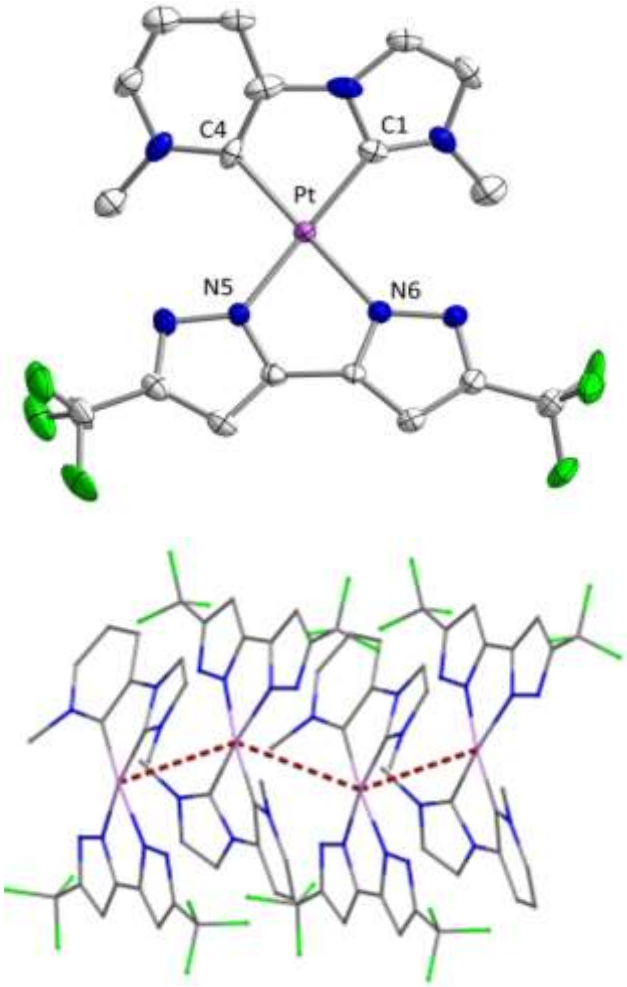

Figure 2. Structural drawing of **2** with thermal ellipsoids shown at the 50% probability level (top). Diagram showing the molecular stacking and Pt···Pt distance of 3.914 Å. Selected bond distances: Pt-C(1) = 1.994(6), Pt-C(4) = 1.992(6), Pt-N(5) = 2.063(5) and Pt-N(6) = 2.058(5) Å, and bond angles: C(1)-Pt-C(4) = 79.1(3) and N(5)-Pt-N(6) = 76.4(19)°.

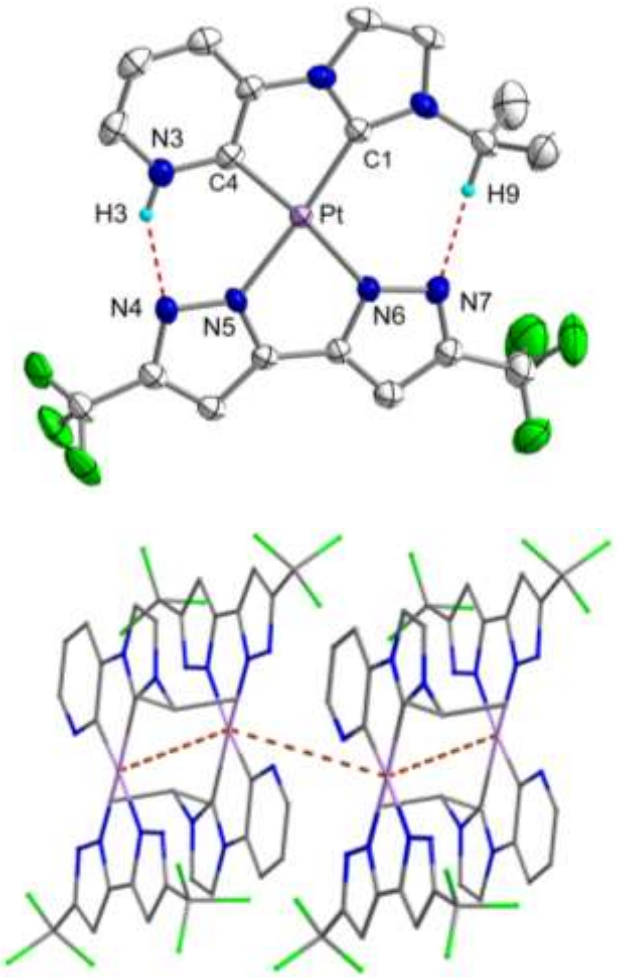

Figure 3. Structural drawing of **5** with thermal ellipsoids shown at the 50% probability level (top). Diagram showing the molecular stacking and Pt···Pt distance of 3.902 Å (bottom). Selected bond distances: Pt-C(1) = 1.994(5), Pt-C(4) = 1.948(5), Pt-N(5) = 2.037(4), Pt-N(6) = 2.079(5), N(4)···H(3) = 2.035(4) and N(7)···H(9) = 2.075(4) Å, and bond angles: C(1)-Pt-C(4) = 79.0(2) and N(5)-Pt-N(6) = 77.4(16)°.

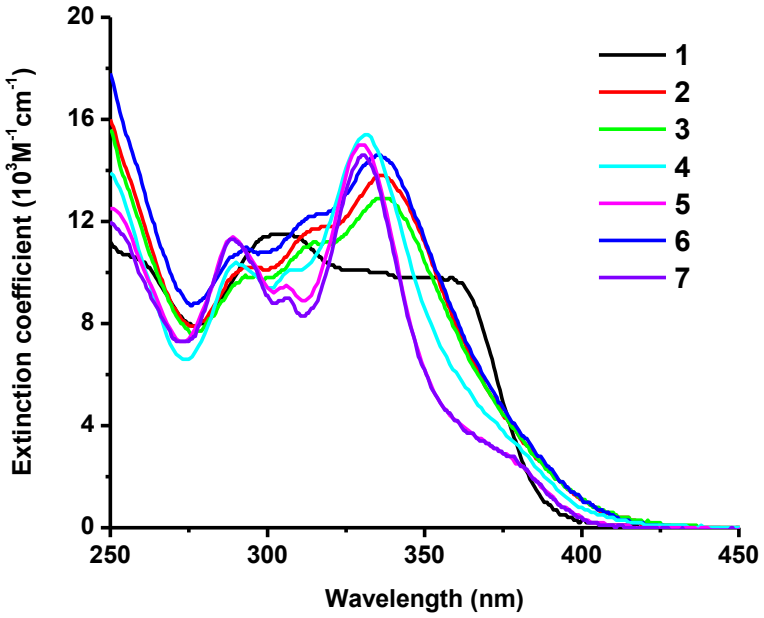

Figure 4. UV-Vis absorption spectra of the studied Pt(II) complexes **1** – **7** recorded in CH_2Cl_2 at RT.

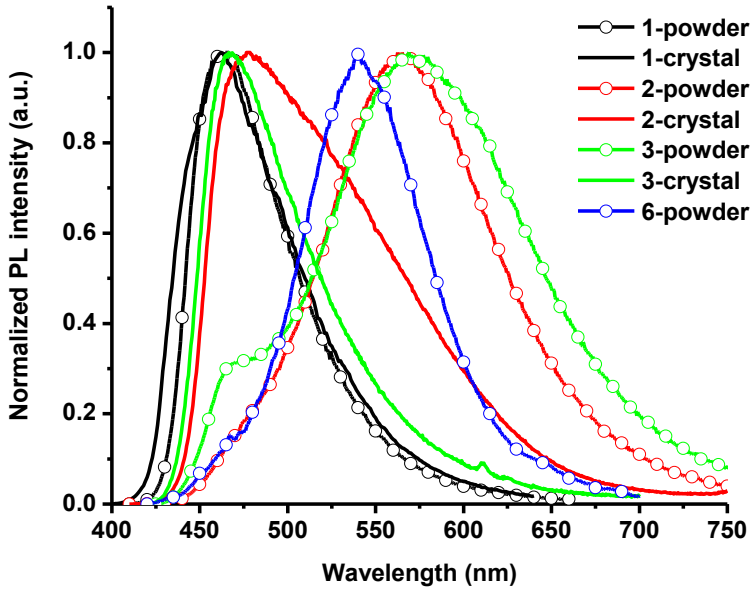

Figure 5. Normalized emission spectra of Pt(II) complexes **1** – **3** and **6** as thin film of polycrystals (solid line) and sublimed fine powder (with circle) at RT.

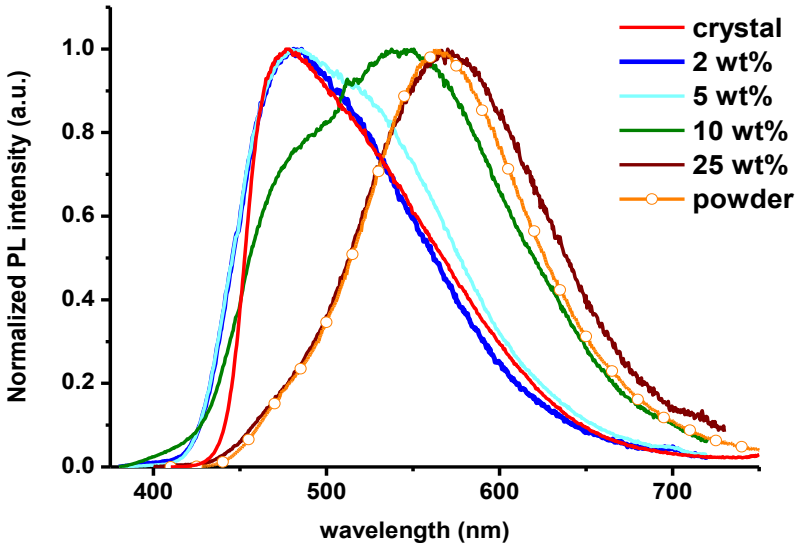

Figure 6. Photoluminescence spectra of the PMMA films with Pt(II) complex **2** varied between 2 wt.% and 25 wt.%, together with that of polycrystalline sample (solid line) and sublimed powder (with circle) as reference.

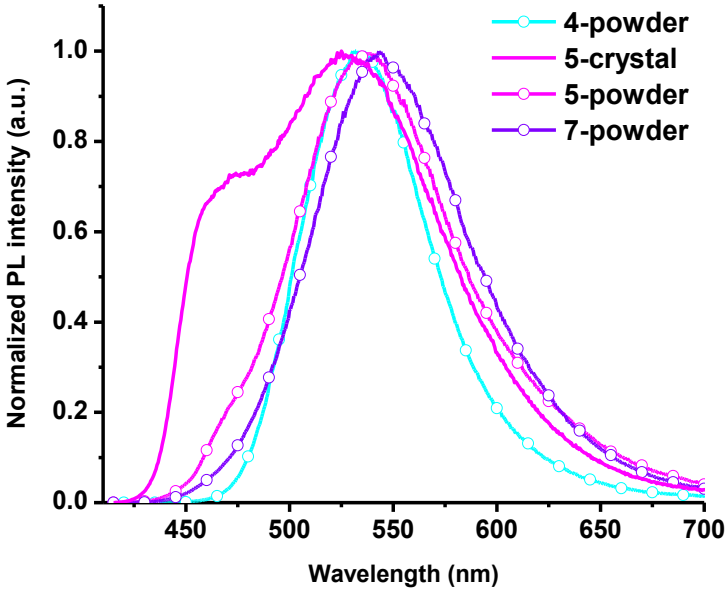

Figure 7. Normalized emission spectra of Pt(II) complexes **4**, **5** and **7** as thin film of polycrystalline sample (solid line) and powder (with circle) at RT.

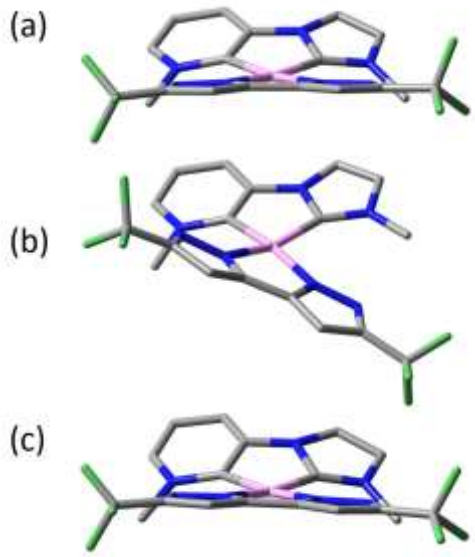

Figure 8. (a) X-ray molecular structure of **2**; (b) optimized geometry of monomer **2**; (c) geometry of middle molecule of **2** in optimized trimer $[\mathbf{2}]_3$.

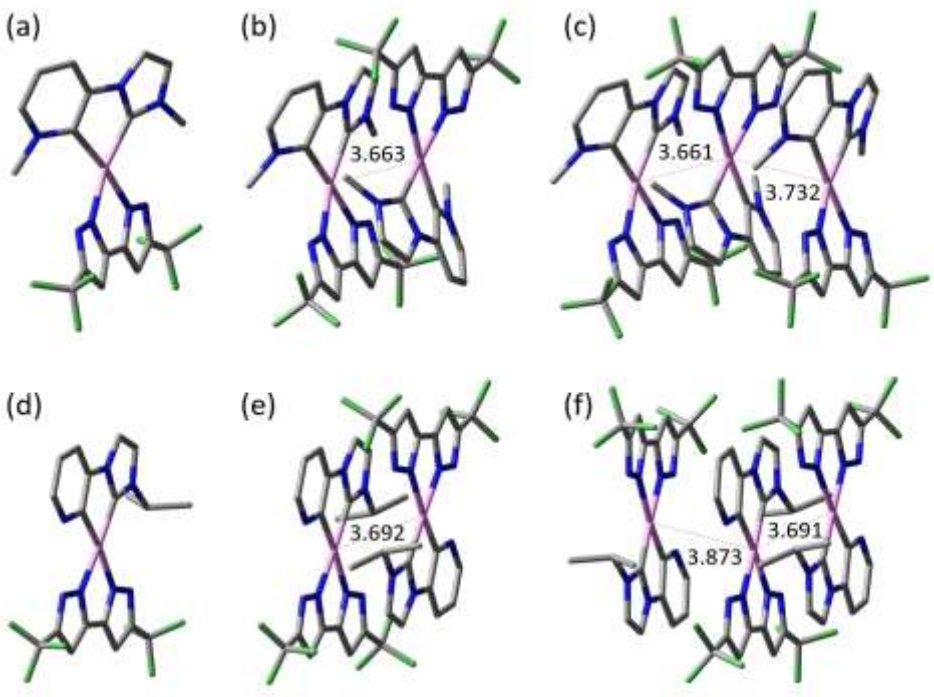

Figure 9. Comparison of the optimized geometries of (a) monomer, (b) dimer and (c) trimer of **2** and (d) monomer, (e) dimer and (f) trimer of **5**, respectively.

	HOMO	LUMO
1	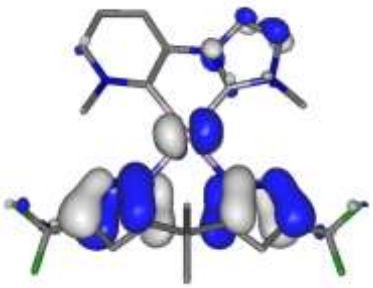	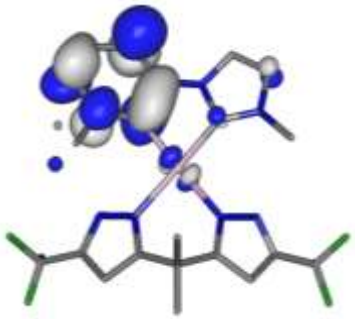
2	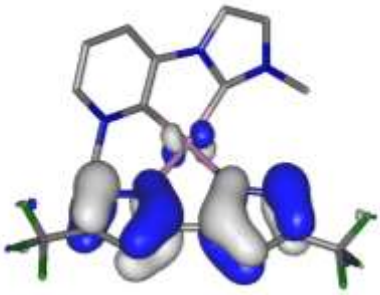	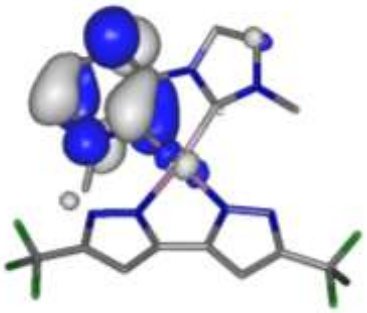
5	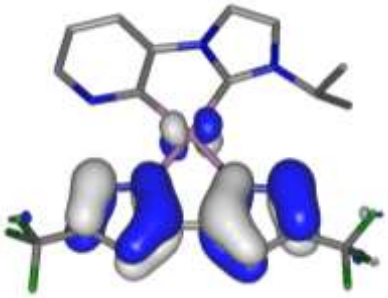	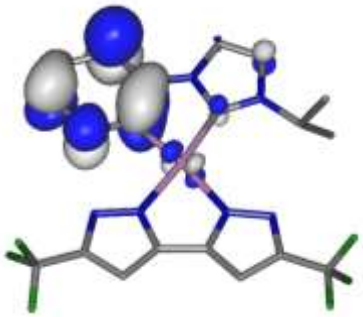

Figure 10. Frontier orbitals for Pt(II) complexes **1**, **2** and **5**.

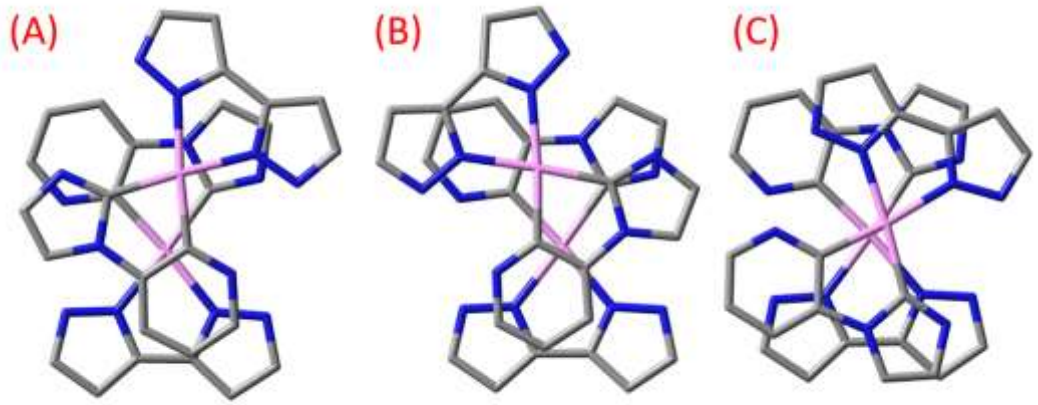

Relative Energy / (kcal mol^{-1})	0.7	0.0	3.6
Pt···Pt (Å)	3.949	3.947	3.197
Relative T_1 Energy	2.4	2.9	0.0
Pt···Pt (Å) T_1	*3.857*	*3.882*	*2.900*

Figure 11. Optimized geometries of three Pt(II) dimers of [**8**]$_2$, A, B and C.

	HOMO	LUMO
B		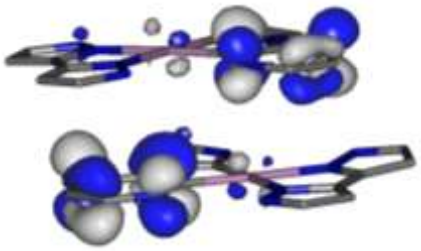
C	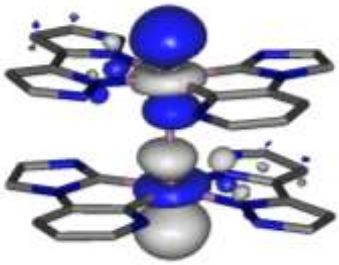	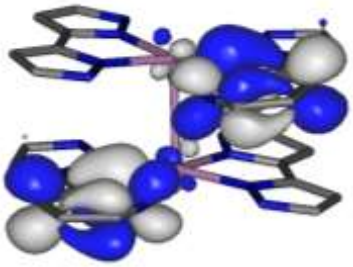

Figure 12. Frontier orbitals on optimized T_1 geometries for dimers of $[\mathbf{8}]_2$, B and C.

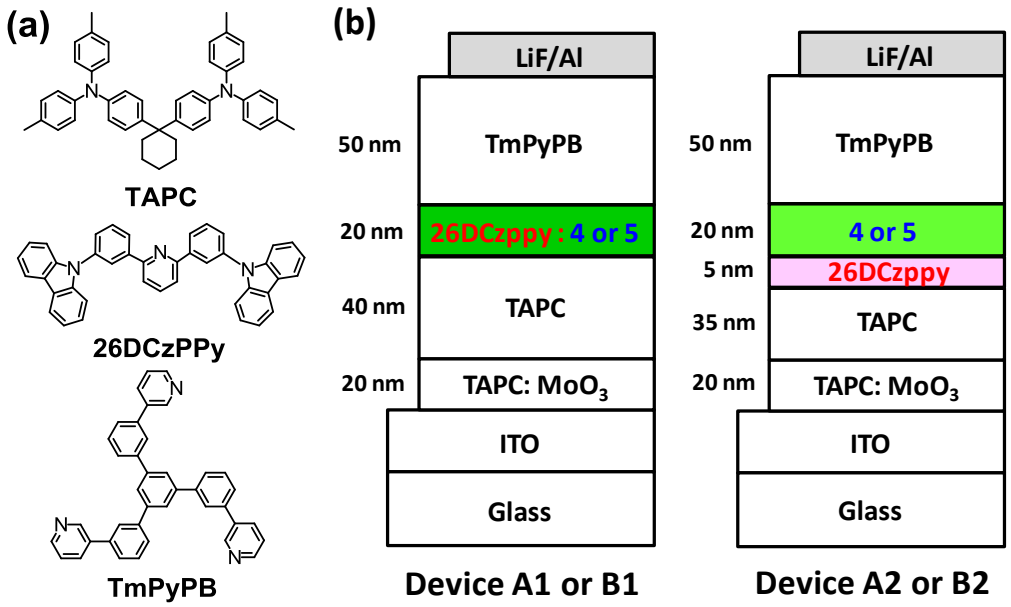

Figure 13. (a) Structural drawing of the materials and (b) schematic structures of the tested OLEDs with Pt(II) phosphors **4** and **5**.

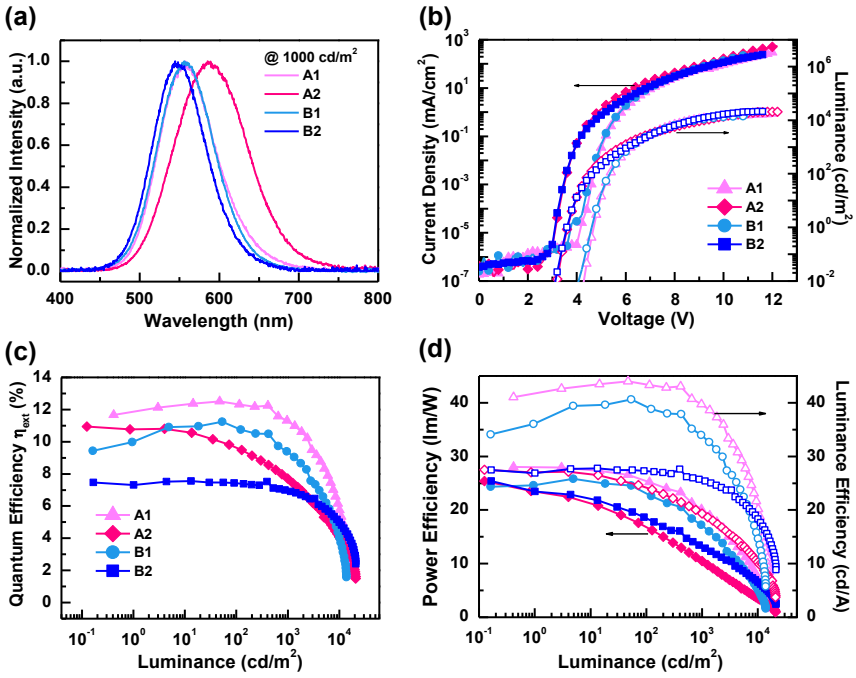

Figure 14. (a) EL spectra of Devices A1, A2, B1 and B2, (b) current density-voltage-luminance (*J-V-L*) characteristics, (c) external quantum efficiency *vs*. luminance, (d) power and luminance efficiencies *vs*. luminance for devices A1, A2, B1

and B2.

Table 1. UV/Vis absorption and emission spectra in solid state and electrochemical data for the studied Pt(II) complexes.

	abs λ_{max} / nm ($\varepsilon \times 10^3$ $M^{-1}\cdot cm^{-1}$)[a]	em λ_{max} (nm)[b]	Φ (%)[b]	τ_{obs} (μs)[b]	E_{pa}^{ox} (V)[c]	E_{pc}^{re} (V)[c]
1	306 (12), 359 (10)	462 [462]	20 [16]	8.97 [7.69]	1.20	-2.14
2	291 (10), 312 (12), 336 (14)	477, 566 [566]	74 [89]	6.98 [1.25]	0.84	-2.12
3	293 (9.9), 315 (11), 336 (13)	468 [468 sh, 569]	17 [24]	4.08 [1.52]	0.86	-2.16
4	290 (11), 331 (15)	[532]	[96]	[0.85]	0.90	-2.22
5	289 (10), 330 (15)	465, 537 [537]	41 [78]	2.37 [0.88]	0.94	-2.23
6	293 (11), 313 (12), 335 (15)	[539]	[0.5]	[0.55]	0.97	-2.16
7	289 (11), 330 (15)	[543]	[99]	[0.84]	0.91	-2.14

[a] UV-Vis spectra were measured in CH_2Cl_2 at 10^{-5} M. [b] PL data of polycrystalline sample and sublimed powder are depicted in standard text format and enclosed in square brackets; sh = shoulder. [c] E_{pa} and E_{pc} are anodic and cathodic peak potentials recorded in CH_2Cl_2 and THF solutions respectively, and the data are quoted with reference to the FcH^+/FcH couple.

Table 2. Comparison of computed MO energies in eV with observed electrochemical data in V for Pt(II) complexes **1**, **2** and **5**.

	Calculated HOMO	Calculated LUMO	Calculated HLG	Observed[a] HOMO	Observed[b] LUMO	Observed HLG
1	-6.20	-2.19	4.01	-6.10	-2.26	3.84
2	-5.79	-2.25	3.54	-5.74	-2.28	3.46
5	-5.88	-2.16	3.72	-5.84	-2.17	3.67

[a] E(HOMO) = - E_{pa} -4.9 V where 5.0 V is the FcH^+/FcH couple in DCM and 0.1 V corrected for the half wave potential of the E_{pa} wave. [b] E(LUMO) = - E_{pc} -4.4 V where 4.3 V is assumed as the FcH^+/FcH couple in THF with the 0.1 V half wave correction for comparison with computed LUMO energies.

Table 3. Comparison of predicted lowest energy absorption and highest energy emission data with observed photophysical data for Pt(II) complexes **1**, **2** and **5**.

	$S_0 \rightarrow S_1$ (nm)	Oscillator Strength (f)	$S_0 \leftarrow T_1$ (nm)	Observed[a] Absorption (nm)	Observed[b] Emission (nm)
1	368	0.0366	459	365	462
2	417	0.0022	479	403	477
5	393	0.0106	465	400	465

[a] Lowest energy absorption minima derived from Gaussian deconvolution analyses, Figure S5. [b] Emission minima from polycrystalline solid state emission data, Figure S6.

Table 4. EL characteristics of tested devices with Pt(II) complexes **4** and **5**.

Device		**A1**	**A2**	**B1**	**B2**
Dopant		**4**		**5**	
concentration (wt.%)		8	100	8	100
External Quantum Efficiency (%)	[a]	12.5	11.0	11.2	7.5
	[b]	12.4	9.6	10.9	7.4
	[c]	11.3	7.7	9.4	7.0
Luminescence Efficiency (cd/A)	[a]	44.0	27.5	40.6	27.5
	[b]	43.4	24.2	39.4	27.3
	[c]	39.7	19.3	33.8	25.6
Power Efficiency (lm/W)	[a]	28.0	25.4	25.8	25.4
	[b]	25.5	16.9	23.2	18.5
	[c]	20.1	10.5	17.1	13.2
V_{on} (V)	[d]	4.6	3.6	4.6	3.6
Max. Luminance (cd/m^2) [Voltage]		17602 [12.0 V]	20679 [12.2 V]	13844 [11.0 V]	21177 [11.6 V]
CIE 1931 coordinates	[b]	(0.41, 0.56)	(0.53, 0.46)	(0.40, 0.56)	(0.36, 0.58)
	[c]	(0.41, 0.56)	(0.53, 0.46)	(0.40, 0.56)	(0.36, 0.58)
EL λ_{Peak} (nm)		558	598	556	545
FWHM (nm)		82.5	102	82.5	81

[a] Maximum efficiencies; [b] those recorded at 10^2 cd/m^2 and [c] at 10^3 cd/m^2; [d] turn-on voltage measured at 1 cd/m^2.

References

1. (a) P.-T. Chou and Y. Chi, *Chem. Eur. J.*, 2007, **13**, 380-395; (b) W.-Y. Wong and C.-L. Ho, *J. Mater. Chem.*, 2009, **19**, 4457-4482; (c) W.-Y. Wong and C.-L. Ho, *Coord. Chem. Rev.*, 2009, **253**, 1709-1758; (d) Y. Chi and P.-T. Chou, *Chem. Soc. Rev.*, 2010, **39**, 638-655; (e) L. Xiao, Z. Chen, B. Qu, J. Luo, S. Kong, Q. Gong and J. Kido, *Adv. Mater.*, 2011, **23**, 926-952; (f) Y. You and W. Nam, *Chem. Soc. Rev.*, 2012, **41**, 7061-7084; (g) C.-L. Ho and W.-Y. Wong, *New J. Chem.*, 2013, **37**, 1665-1683; (h) H. Xiang, J. Cheng, X. Ma, X. Zhou and J. J. Chruma, *Chem. Soc. Rev.*, 2013, **42**, 6128-6185; (i) L. Ying, C.-L. Ho, H. Wu, Y. Cao and W.-Y. Wong, *Adv. Mater.*, 2014, **26**, 2459-2473; (j) X. Yang, G. Zhou and W.-Y. Wong, *J. Mater. Chem. C*, 2014, **2**, 1760-1778; (k) X. Yang, G. Zhou and W.-Y. Wong, *Chem. Soc. Rev.*, 2015, **44**, 8484-8575; (l) X. Xu, X. Yang, J. Zhao, G. Zhou and W.-Y. Wong, *Asian J. Org. Chem.*, 2015, **4**, 394-429; (m) C.-W. Lu, Y. Wang and Y. Chi, *Chem. Eur. J.*, 2016, **22**, 17892-17908; (n) Y. Chi, T.-K. Chang, P. Ganesan and P. Rajakannu, *Coord. Chem. Rev.*, 2017, doi: 10.1016/j.ccr.2016.1011.1016.

2. (a) W.-Y. Wong, Z. He, S.-K. So, K.-L. Tong and Z. Lin, *Organometallics*, 2005, **24**, 4079-4082; (b) Z. He, W.-Y. Wong, X. Yu, H.-S. Kwok and Z. Lin, *Inorg. Chem.*, 2006, **45**, 10922-10937; (c) J. A. G. Williams, S. Develay, D. L. Rochester and L. Murphy, *Coord. Chem. Rev.*, 2008, **252**, 2596-2611; (d) J. A. G. Williams, *Chem. Soc. Rev.*, 2009, **38**, 1783-1801; (e) G. Zhou, Q. Wang, C.-L. Ho, W.-Y. Wong, D. Ma and L. Wang, *Chem. Commun.*, 2009, 3574-3576; (f) L. Murphy and J. A. G. Williams, *Top. Organomet. Chem.*, 2010, **28**, 75; (g) G. Zhou, Q. Wang, X. Wang, C.-L. Ho, W.-Y. Wong, D. Ma, L. Wang and Z. Lin, *J. Mater. Chem.*, 2010, **20**, 7472-7484; (h) G. Tan, S. Chen, N. Sun, Y. Li, D. Fortin, W.-Y. Wong, H.-S. Kwok, D. Ma, H. Wu, L. Wang and P. D. Harvey, *J. Mater. Chem. C*, 2013, **1**, 808-821; (i) G. Tan, S. Chen, C.-H. Siu, A. Langlois, Y. Qiu, H. Fan, C.-L. Ho, P. D. Harvey, Y.-H. Lo, L. Liu and W.-Y. Wong, *J. Mater. Chem. C*, 2016, **2**, 6016-6026.

3. (a) G. Cheng, P.-K. Chow, S. C. F. Kui, C.-C. Kwok and C.-M. Che, *Adv. Mater.*, 2013, **25**, 6765-6770; (b) K. Li, G. Cheng, C. Ma, X. Guan, W.-M. Kwok, Y. Chen, W. Lu and C. M. Che, *Chem. Sci.*, 2013, **4**, 2630-2644; (c) X.-C. Hang, T. Fleetham, E. Turner, J. Brooks and J. Li, *Angew. Chem. Int. Ed.*, 2013, **52**, 6753-6756; (d) T. Fleetham, G. Li and J. Li, *ACS Appl. Mater. Interfaces*, 2015, **7**, 16240-16246; (e) B. Wang, F. Liang, H. Hu, Y. Liu, Z. Kang, L.-S. Liao and J. Fan, *J. Mater. Chem. C*, 2015, **3**, 8212-8218.

4. (a) J.-L. Chen, S.-Y. Chang, Y. Chi, K. Chen, Y.-M. Cheng, C.-W. Lin, G.-H. Lee, P.-T. Chou, C.-H. Wu, P.-I. Shih and C.-F. Shu, *Chem. Asian J.*, 2008, **3**, 2112-2123; (b) Z. Wang, E. Turner, V. Mahoney, S. Madakuni, T. Groy and J. Li, *Inorg. Chem.*, 2010, **49**, 11276-11286; (c) W. Mroz, C. Botta, U. Giovanella, E. Rossi, A. Colombo, C. Dragonetti, D. Roberto, R. Ugo, A. Valore and J. A. G. Williams, *J. Mater. Chem.*, 2011, **21**, 8653; (d) T. Fleetham, J. Ecton, Z. Wang, N. Bakken and J. Li, *Adv. Mater.*, 2013, **25**, 2573-2576; (e) T. Kayano, S. Takayasu, K. Sato and K. Shinozaki, *Chem. Eur. J.*, 2014, **20**, 16583-16589; (f) P.-K. Chow, G. Cheng, G. S. M. Tong, W.-P. To, W.-L. Kwong, K.-H. Low, C.-C. Kwok, C. Ma and C.-M. Che, *Angew. Chem. Int. Ed.*, 2015, **54**, 2084-2089.

5. (a) B. Ma, P. I. Djurovich, M. Yousufuddin, R. Bau and M. E. Thompson, *J. Phys. Chem. C*, 2008, **112**, 8022; (b) S.-Y. Chang, Y.-M. Cheng, Y. Chi, Y.-C. Lin, C.-M. Jiang, G.-H. Lee and P.-T. Chou, *Dalton Trans.*, 2008, 6901-6911; (c) P. Brulatti, V. Fattori, S. Muzzioli, S. Stagni, P. P. Mazzeo, D. Braga, L. Maini, S. Milita and M. Cocchi, *J. Mater. Chem. C*, 2013, **1**, 1823-1831; (d) M. Micutz,

M. Ilis, T. Staicu, F. Dumitrascu, I. Pasuk, Y. Molard, T. Roisnel and V. Circu, *Dalton Trans.*, 2014, **43**, 1151-1161; (e) M. Tanaka and H. Mori, *J. Phys. Chem. C*, 2014, **118**, 12443-12449; (f) K. Li, G. S. Ming Tong, Q. Wan, G. Cheng, W.-Y. Tong, W.-H. Ang, W.-L. Kwong and C.-M. Che, *Chem. Sci.*, 2016, **7**, 1653-1673.

6. L. Murphy, P. Brulatti, V. Fattori, M. Cocchi and J. A. G. Williams, *Chem. Commun.*, 2012, **48**, 5817-5819.

7. (a) Y. Chi, B. Tong and P.-T. Chou, *Coord. Chem. Rev.*, 2014, **281**, 1-25; (b) S.-Y. Chang, J. Kavitha, S.-W. Li, C.-S. Hsu, Y. Chi, Y.-S. Yeh, P.-T. Chou, G.-H. Lee, A. J. Carty, Y.-T. Tao and C.-H. Chien, *Inorg. Chem.*, 2006, **45**, 137-146; (c) S.-Y. Chang, J. Kavitha, J.-Y. Hung, Y. Chi, Y.-M. Cheng, E. Y. Li, P.-T. Chou, G.-H. Lee and A. J. Carty, *Inorg. Chem.*, 2007, **46**, 7064-7074; (d) L.-M. Huang, G.-M. Tu, Y. Chi, W.-Y. Hung, Y.-C. Song, M.-R. Tseng, P.-T. Chou, G.-H. Lee, K.-T. Wong, S.-H. Cheng and W.-S. Tsai, *J. Mater. Chem. C*, 2013, **1**, 7582-7592; (e) H.-Y. Ku, B. Tong, Y. Chi, H.-C. Kao, C.-C. Yeh, C.-H. Chang and G.-H. Lee, *Dalton Trans.*, 2015, **44**, 8552-8563; (f) K. T. Ly, R.-W. Chen-Cheng, H.-W. Lin, Y.-J. Shiau, S.-H. Liu, P.-T. Chou, C.-S. Tsao, Y.-C. Huang and Y. Chi, *Nat. Photon.*, 2016, DOI: 10.1038/NPHOTON.2016.1230.

8. (a) X. Wang, Y.-L. Chang, J.-S. Lu, T. Zhang, Z.-H. Lu and S. Wang, *Adv. Funct. Mater.*, 2014, **24**, 1911-1927; (b) X. Wang, S.-L. Gong, D. Song, Z.-H. Lu and S. Wang, *Adv. Funct. Mater.*, 2014, **26**, 7257-7271.

9. C.-W. Hsu, Y. Zhao, H.-H. Yeh, C.-W. Lu, C. Fan, Y. Hu, N. Robertson, G.-H. Lee, X. Sun and Y. Chi, *J. Mater. Chem. C*, 2015, **3**, 10837-10847.

10. C. W. Hsu, K. T. Ly, W.-K. Lee, C.-C. Wu, L.-C. Wu, J.-J. Lee, T.-C. Lin, S.-H. Liu, P.-T. Chou, G.-H. Lee and Y. Chi, *ACS Appl. Mater. Interfaces*, 2016, **8**, 33888-33898.

11. (a) R. Visbal and M. C. Gimeno, *Chem. Soc. Rev.*, 2014, **43**, 3551-3574; (b) J.-L. Liao, Y. Chi, J.-Y. Wang, Z.-N. Chen, Z.-H. Tsai, W.-Y. Hung, M.-R. Tseng and G.-H. Lee, *Inorg. Chem.*, 2016, **55**, 6394-6404.

12. (a) S. Gomez-Bujedo, M. Alcarazo, C. Pichon, E. Alvarez, R. Fernandez and J. M. Lassaletta, *Chem. Commun.*, 2007, 1180-1182; (b) G. Song, Y. Zhang, Y. Su, W. Deng, K. Han and X. Li, *Organometallics*, 2008, **27**, 6193-6201; (c) A. McSkimming, G. E. Ball, M. M. Bhadbhade and S. B. Colbran, *Inorg. Chem.*, 2012, **51**, 2191-2203.

13. C. Segarra, E. Mas-Marzá, J. A. Mata and E. Peris, *Organometallics*, 2012, **31**, 5169-5176.

14. (a) A. D. Becke, *J. Chem. Phys.*, 1993, **98**, 5648-5652; (b) P. J. Stephens, F. J. Devlin, C. F. Chabalowski and M. J. Frisch, *J. Phys. Chem.*, 1994, **98**, 11623-11627.

15. D. Andrae, U. Häußermann, M. Dolg, H. Stoll and H. Preuß, *Theor. Chim. Acta*, 1990, **77**, 123-141.

16. G. A. Petersson and M. A. Al-Laham, *J. Chem. Phys.*, 1991, **94**, 6081-6090.

17. S. Grimme, J. Antony, S. Ehrlich and H. Krieg, *J. Chem. Phys*, 2010, **132**, 154104.

18. M. Cossi and V. Barone, *J. Chem. Phys.*, 2001, **115**, 4708-4717.

19. N. M. O'Boyle, A. L. Tenderholt and K. M. Langner, *J. Comput. Chem.*, 2008, **29**, 839-845.

20. (a) K. Li, X. Guan, C.-W. Ma, W. Lu, Y. Chen and C.-M. Che, *Chem. Commun.*, 2011, **47**, 9075-9077; (b) S. Fuertes, H. García, M. Perálvarez, W. Hertog, J. Carreras and V. Sicilia, *Chem. Eur. J.*, 2015, **21**, 1620-1631; (c) A. Tronnier, U. Heinemeyer, S. Metz, G. Wagenblast, I. Muenster and T. Strassner, *J. Mater. Chem. C*, 2015, **3**, 1680-1693; (d) A. R. Naziruddin, A. Galstyan, A. Iordache, C. G. Daniliuc, C. A. Strassert and L. De Cola, *Dalton Trans.*, 2015, **44**, 8467-8477.

21. (a) L. Holland, W.-Z. Shen, P. von Grebe, P. J. Sanz Miguel, F. Pichierri, A. Springer, C. A. Schalley and B. Lippert, *Dalton Trans.*, 2011, **40**, 5159-5161; (b) X.-H. Zhao, G.-H. Xie, Z.-D. Liu, W.-J. Li, M.-d. Yi, L.-H. Xie, C.-P. Hu, R. Zhu, Q. Zhao, Y. Zhao, J.-F. Zhao, Y. Qian and W. Huang, *Chem. Commun.*, 2012, **48**, 3854-3856; (c) S.-B. Ko, J.-S. Lu, Y. Kang and S. Wang, *Organometallics*, 2013, **32**, 599; (d) H. Uesugi, T. Tsukuda, K. Takao and T. Tsubomura, *Dalton Trans.*, 2013, **42**, 7396-7403; (e) H. Li, W. Yuan, X. Wang, H. Zhan, Z. Xie and Y. Cheng, *J. Mater. Chem. C*, 2015, **3**, 2744-2750.

22. (a) D. P. Rillema, A. J. Cruz, C. Moore, K. Siam, A. Jehan, D. Base, T. Nguyen and W. Huang, *Inorg. Chem.*, 2013, **52**, 596-607; (b) J.-L. Liao, Y. Chi, S.-H. Liu, G.-H. Lee, P.-T. Chou, H.-X. Huang, Y.-D. Su, C.-H. Chang, J.-S. Lin and M.-R. Tseng, *Inorg. Chem.*, 2014, **53**, 9366-9374; (c) J.-L. Liao, Y. Chi, C.-C. Yeh, H.-C. Kao, C.-H. Chang, M. A. Fox, P. J. Low and G.-H. Lee, *J. Mater. Chem. C*, 2015, **3**, 4910-4920.

23. (a) A. F. Rausch, L. Murphy, J. A. G. Williams and H. Yersin, *Inorg. Chem.*, 2012, **51**, 312-319; (b) B.-S. Du, J.-L. Liao, M.-H. Huang, C.-H. Lin, H.-W. Lin, Y. Chi, H.-A. Pan, G.-L. Fan, K.-T. Wong, G.-H. Lee and P.-T. Chou, *Adv. Funct. Mater.*, 2012, **22**, 3491-3499.

24. (a) V. M. Miskowski and V. H. Houlding, *Inorg. Chem.*, 1991, **30**, 4446-4452; (b) V. W.-W. Yam, K. M.-C. Wong and N. Zhu, *J. Am. Chem. Soc.*, 2002, **124**, 6506; (c) W. Lu, M. C. W. Chan, N. Zhu, C.-M. Che, C. Li and Z. Hui, *J. Am. Chem. Soc.*, 2004, **126**, 7639; (d) A. l. Díez, J. Forniés, C. Larraz, E. Lalinde, J. A. López, A. Martín, M. T. Moreno and V. Sicilia, *Inorg. Chem.*, 2010, **49**, 3239-3251; (e) J. S. Field, C. D. Grimmer, O. Q. Munro and B. P. Waldron, *Dalton Trans.*, 2010, **39**, 1558; (f) Y. Nishiuchi, A. Takayama, T. Suzuki and K. Shinozaki, *Eur. J. Inorg. Chem.*, 2011, 1815; (g) C.-T. Liao, H.-H. Chen, H.-F. Hsu, A. Poloek, H.-H. Yeh, Y. Chi, K.-W. Wang, C.-H. Lai, G.-H. Lee, C.-W. Shih and P.-T. Chou, *Chem. Eur. J.*, 2011, **17**, 546; (h) V. Sicilia, J. Fornies, J. M. Casas, A. Martin, J. A. Lopez, C. Larraz, P. Borja, C. Ovejero, D. Tordera and H. Bolink, *Inorg. Chem.*, 2012, **51**, 3427; (i) C. Cuerva, J. A. Campo, P. Ovejero, M. R. Torres, E. Oliveira, S. M. Santos, C. Lodeiro and M. Cano, *J. Mater. Chem. C*, 2014, **2**, 9167-9181; (j) A. Amar, H. Meghezzi, J. Boixel, H. Le Bozec, V. Guerchais, D. Jacquemin and A. Boucekkine, *J. Phys. Chem. A*, 2014, **118**, 6278-6286.

25. J. Romanova, M. R. Ranga Prabhath and P. D. Jarowski, *J. Phys. Chem. C*, 2016, **120**, 2002-2012.

26. (a) E. Rossi, A. Colombo, C. Dragonetti, D. Roberto, F. Demartin, M. Cocchi, P. Brulatti, V. Fattori and J. A. G. Williams, *Chem. Commun.*, 2012, **48**, 3182-3184; (b) X.-P. Zhang, J.-F. Mei, J.-C. Lai, C.-H. Li and X.-Z. You, *J. Mater. Chem. C*, 2015, **3**, 2350-2357.

27. (a) X. Wang, Y. Li, L. Wang and J. Zhang, *Org. Electron.*, 2016, **35**, 208-215; (b) K.-H. Kim, J.-L. Liao, S. W. Lee, B. Sim, C.-K. Moon, G.-H. Lee, H. J. Kim, Y. Chi and J.-J. Kim, *Adv. Mater.*, 2016, **28**, 2526-2532.

28. H. Matsushima, S. Naka, H. Okada and H. Onnagawa, *Curr. Appl. Phys.*, 2005,

5, 305-308.

29. R. J. Holmes, S. R. Forrest, Y.-J. Tung, R. C. Kwong, J. J. Brown, S. Garon and M. E. Thompson, *Appl. Phys. Lett.*, 2003, **82**, 2422.

30. S.-J. Su, H. Sasabe, T. Takeda and J. Kido, *Chem. Mater.*, 2008, **20**, 1691.

31. (a) K. Goushi, R. Kwong, J. J. Brown, H. Sasabe and C. Adachi, *J. Appl. Phys.*, 2004, **95**, 7798; (b) S.-J. Su, T. Chiba, T. Takeda and J. Kido, *Adv. Mater.*, 2008, **20**, 2125.

32. C. Cai, S.-J. Su, T. Chiba, H. Sasabe, Y.-J. Pu, K. Nakayama and J. Kido, *Org. Electron.*, 2011, **12**, 843-850.

33. S. Hamwi, J. Meyer and T. Winkler, *Appl. Phys. Lett.*, 2009, **94**, 253307-253307.

34. Y. Hong, J. W. Y. Lam and B. Z. Tang, *Chem. Soc. Rev.*, 2011, **40**, 5361-5388.

35. W. C. Wu, H. C. Yeh, L. H. Chan and C. T. Chen, *Adv. Mater.*, 2002, **14**, 1072-1075.

36. C.-L. Lin, H.-W. Lin and C.-C. Wu, *Appl. Phys. Lett.*, 2005, **87**, 021101.

37. M. A. Baldo, C. Adachi and S. R. Forrest, *Phys. Rev. B.*, 2000, **62**, 10967.

38. J. Kalinowski, M. Cocchi, V. Fattori, L. Murphy and J. A. G. Williams, *Org. Electron.*, 2010, **11**, 724-730.